→ Biopolymers
→ Molecular Motors and Filaments
→ Ribosomes and Protein Synthesis
→ Membranes and Vesicles
→ Interfacial Phenomena
→ Complex Systems

THEORY & BIO-SYSTEMS

Research in the Department of Theory & Bio-Systems

Denken ohne Erfahrung ist leer, Erfahrung ohne Denken ist blind.
Immanuel Kant

The main objective of our research activities is to understand the hidden dimensions of self-organization in biomimetic and biological systems. The molecular building blocks of these systems join „by themselves" and form a variety of supra-molecular assemblies, which then interact to produce even larger structures and networks.

Reinhard Lipowsky 11.11.1953
1978: Diploma, Physics, (University of Heidelberg)
1982: PhD (Dr. rer. nat.), Physics (University of Munich)
1979-1984: Teaching Associate (University of Munich)
1984-1986: Research Associate (Cornell University)
1986-1988: Group leader (FZ Jülich)
1987: Habilitation, Theoretical Physics (University of Munich)
Thesis: Critical behavior of interfaces: Wetting, surface melting and related phenomena
1989-1990: Associate Professorship (University of Munich)
1990-1993: Full Professorship (University of Cologne), Director of the Division "Theory II" (FZ Jülich)
Since Nov 1993: Director (Max Planck Institute of Colloids and Interfaces, Potsdam)

The associates of the department form several research groups. At present, the research group leaders and topics are:

· *Rumiana Dimova:* Biophysics Lab;
· *Thomas Weikl:* Proteins and Membranes;
· *Mark Santer:* Carbohydrates and Polysaccharides;
· *Christian Seidel:* Polymers and Polyelectrolytes;
· *Andrea Grafmüller:* Multiscale Simulations;
· *Angelo Valleriani:* Stochastic Processes;
· *Stefan Klumpp:* Regulation of Bioprocesses.

The main results of these research groups are described in separate reports on the following pages. These reports are ordered in a bottom-up manner, i.e., from small to large length scales, and related to five research areas: Biopolymers, Motors and Filaments, Membranes and Vesicles, Soft Interfaces, and Complex Systems. Here, the results of the research groups will be briefly summarized and some additional results will be highlighted.

Biopolymers

Carbohydrates and polysaccharides have been studied by the research group of *M. Santer* using molecular dynamics simulations. The focus was on two types of polysaccharides: GPI-anchors, which can link a variety of proteins to cell membranes, and lipopolysaccharides, which protect bacteria against the infection by bacteriophages. The conformational freedom of the different glycosidic bonds between the subunits of the polysaccharides was determined by calculating free energy landscapes as a function of glycosidic torsion angles: even short oligosaccharides were shown to be relatively flexible.

Proteins that act as enzymes must first bind the reaction partners as ligands. The group of *T. Weikl* considered the temporal ordering of these binding processes with respect to conformational changes of the enzymes: the enzyme may undergo conformational changes before ligand binding or the ligands may first bind and then induce conformational changes of the enzyme. The temporal ordering has no effect on the binding equilibrium, but affects the binding kinetics and, thus, may be revealed by mutations of the protein.

Molecular Motors and Filaments

Intracellular cargo is transported by teams of molecular motors that pull on the cargo via elastic stalks. The simplest case corresponds to cooperative transport by two identical motors as shown in **Fig. 1**. The influence of this elastic coupling between the motors on the transport properties has been addressed in the framework of chemomechanical networks and semistochastic models (see the report by *F. Berger* and *C. Keller*). The chemomechanical networks are relatively complex but involve only two additional parameters that can be deduced from the cargo trajectories. The semi-stochastic models reveal different interference regimes, in which the motors stall each other or pull each other from the filament.

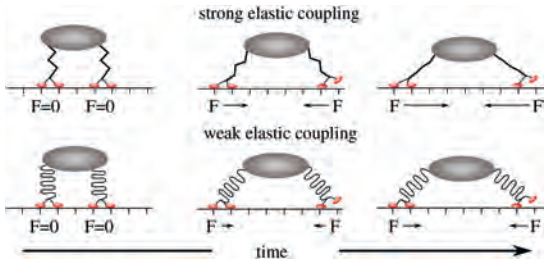

Fig.1: Two molecular motors coupled to a cargo particle via their elastic stalks or linkers. The motors step forward stochastically and stretch their linkers, thereby inducing an elastic interaction that generates the mutual strain force F. Strong elastic coupling leads to a fast buildup of large forces, whereas weakly coupled motors experience only relatively small forces. [F. Berger et al, Phys. Rev. Lett. (2012)]

Another molecular motor, for which a chemo-mechanical network has been constructed, is myosin V that steps along actin filaments, see **Fig 2**. Furthermore, stochastic tug-of-wars between two teams of molecular motors were experimentally confirmed for the transport of early endosomes in fungi. In this case, dyneins that bind to a cargo or unbind from it can change the cargo's direction of motion, see **Fig 3**.

In the context of actin filaments, we have addressed a recent controversy about the depolymerization of actin filaments (see the report by *T. Niedermayer*). Using single filament experiments, it was shown that the depolymerization of actin filaments typically proceeds in a bi-phasic way, with an initial fast phase interrupted by a slow phase, see **Fig. 4**. In contrast to previous proposals, the interruptions were shown to be caused by the local and random dimerization of actin subunits. The theoretical analysis of the stochastic interruption times and pause durations provides a general method to determine rather small changes in the molecular interactions between the subunits of actin filaments.

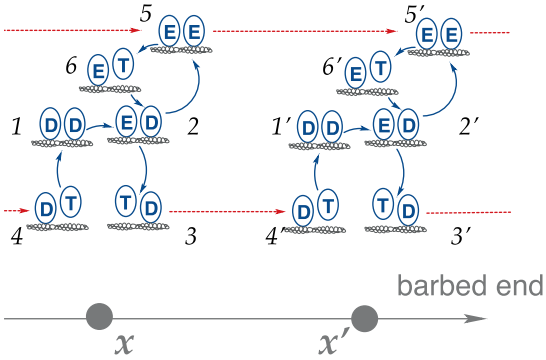

Fig. 2: Chemomechanical network for myosin V that steps along actin filaments. At each filament position x, x′,..., the chemical network of the motor consists of six states. The motor can perform two types of mechanical forward steps, l34′) and l55′), towards the barbed end of the filament. [V. Bierbaum et al, Biophys. J. (2011); PLoS ONE (2013)]

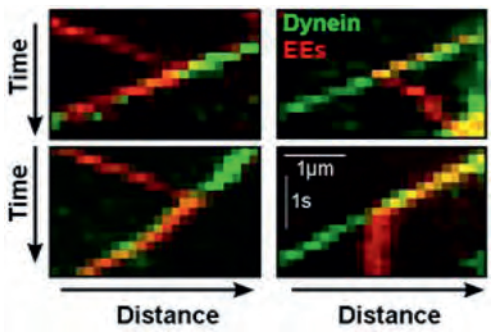

Fig 3: Changes in the direction of motion for red-labeled cargo particles by green-labeled dynein motors that bind to (left) or unbind from (right) the cargo. [M. Schuster et al, PNAS (2011)]

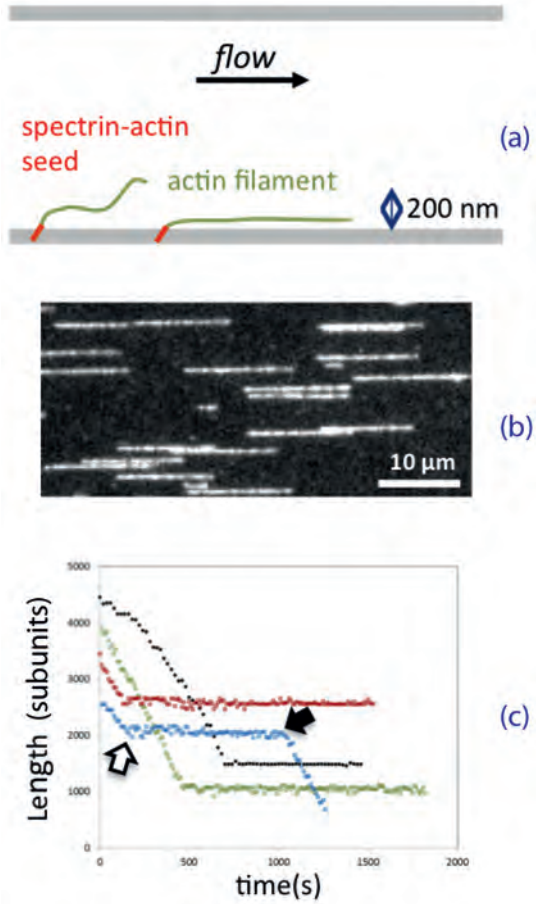

Fig.4: (a) Actin filaments are anchored to the chamber wall and aligned by a continuous microfluidic flow. Actin depolymerization is induced by fast switching to a flow channel without actin; (b) The filaments are imaged using TIRF or epifluorescence microscopy; and (c) The length of the filaments as measured during depolymerization; black data points correspond to a filament grown from MgATP-actin whereas red, green, and blue data points were obtained for three filaments grown from MgADP-actin. One pause in depolymerization occurs between the white and black arrow in (c). [T. Niedermayer et al, PNAS (2012)]

Ribosomes and Protein Synthesis

Ribosomes are rather complex molecular machines that synthesize proteins by translating the codon sequences of mRNA molecules into peptide chains. In order to do so, the ribosomes move along the mRNAs and translate one codon after another by binding and processing cognate tRNA molecules that are charged with the correct amino acids.

In order to understand this process of translational elongation, one has to take two important molecular features into account. First, the ribosome has three binding pockets for tRNA molecules, the A-, P-, and E-sites, see **Fig. 5**(a). As indicated in this figure, these three sites are aligned along the mRNA that is translated by the ribosome. Second, a tRNA can only bind to the ribosome after it has formed a ternary complex with an EF-Tu protein and a GTP nucleotide, see **Fig. 5**(b).

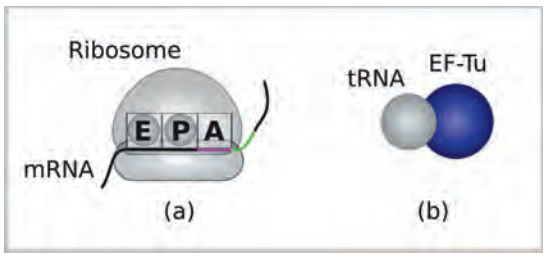

Fig.5: (a) Schematic view of a ribosome (grey dumbbell) that translates a mRNA molecule (black strand). The ribosome has three binding pockets for tRNA molecules, the A-, P-, and E-sites. These three sites are aligned along the mRNA and their separations are equal to the length of a single codon; (b) Ternary complex formed by a tRNA molecule (small grey ball), an EF-Tu protein (large blue ball), and a GTP nucleotide (not shown).

Each tRNA molecule that is processed by the ribosome first binds as a ternary complex to the A-site and is then translocated from the A- to the P-site. During the next elongation cycle, this tRNA is moved from the P- to the E-site, from which it is finally released.

A single, codon-specific cycle of translational elongation involves several ribosomal states as depicted schematically in **Fig 6**. At the beginning of the elongation cycle, the ribosome contains two tRNA molecules in its P- and its E-site but has an empty A-site, which is located at the codon to be translated. In **Fig. 6**, this codon is colored in red. When a cognate tRNA molecule arrives at the ribosome by diffusion, it first binds loosely to the A-site but becomes fully accommodated into this site after its correct anticodon has been recognized. During the latter substeps, the E-site tRNA and the EF-Tu molecule are released from the ribosome and a new peptide bond is formed. However, before the translating ribosome is able to bind and process a cognate tRNA, it typically samples through a large number of noncognate tRNAs that also bind to the ribosomal A-site and, thus, impede binding of the cognate tRNA, see upper left cartoon in **Fig. 6**.

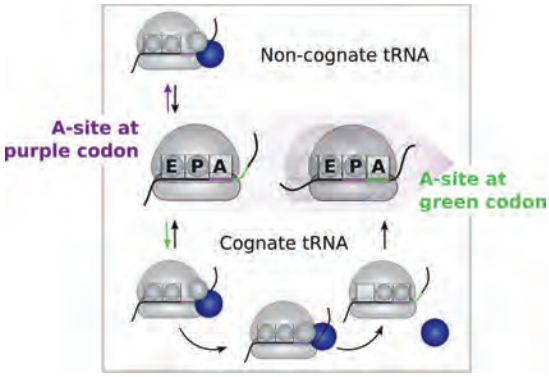

Fig.6: Elongation cycle of a ribosome corresponding to the translation of a single codon (red mRNA segment): Initially, the ribosome dwells at this codon with an empty A-site until a ternary complex arrives and occupies this site. This ternary complex is typically non-cognate (upper left cartoon) and is then released from the A-site without further processing. If a cognate ternary complex is bound (lower left cartoon), it is recognized by its anticodon and is then fully accommodated into the A-site (lower right cartoon). During this accommodation step, the EF-Tu molecule is released. After the formation of a new peptide bond (not shown), the ribosome undergoes translocation and moves to the subsequent codon (green mRNA segment) in order to start the next elongation cycle. [S. Rudorf et al, to be published]

We have recently developed a quantitative theory that takes both the formation of ternary complexes and the competitive binding between cognate and non-cognate tRNAs into account and allows to calculate the codon-specific elongation times of the ribosome. Another interesting aspect of translation that we studied theoretically is the robustness of protein synthesis with respect to variations of individual tRNA concentrations.

Membranes and Vesicles

Lipid molecules in aqueous solution self-assemble into bilayer membranes that have a thickness of about 4nm. In order to desorb from the membrane again, a single lipid has to overcome a large free energy barrier that has been determined in the group of *A. Grafmüller* using atomistic molecular dynamics simulations. Unexpectedly, the desorption free energy was found to increase with membrane tension because of the conformational entropy of the lipid tails.

Lipid vesicles exposed to different aqueous phases exhibit unusual morphologies and morphological transitions as discovered in the group of *R. Dimova*: wetting transitions, droplet-induced budding processes, and spontaneous tubulation, i.e., the formation of membrane nanotubes that are stable even in the absence of external forces. The latter process provides direct evidence that the polymer/lipid interactions lead to a spontaneous membrane curvature that generates a large membrane tension. In fact, one unique feature of aqueous phase separation in vesicles is the possibility to directly determine the membrane tensions from the (effective) contact angles as visible in the optical microscope, see **Fig. 7**, and from the interfacial tension between the two liquid phases.

The interactions of nanoparticles with membranes and vesicles have been studied by the group of *T. Weikl* using Monte Carlo methods to minimize the free energy of the membrane/particle systems. These studies revealed strongly attractive interactions between nanoparticles adsorbed onto vesicles. As a result of these interactions, the adhering nanoparticles aggregate on the vesicle membranes and often form linear chains enwrapped by membrane nanotubes.

Another membrane system that has been addressed is provided by double-membrane structures that play an important role in cellular processes such as autophagy, reproduction, and viral infection. In these processes, one typically starts from double-membrane sheets that become unstable and close up into double-membrane vesicles. The stability of a double-membrane sheet depends primarily on its lateral size and the spontaneous membrane curvature along its rim [R. Knorr et al, PLoS ONE (2012)].

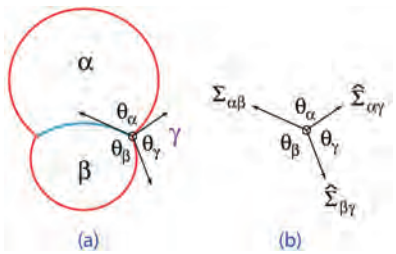

Fig.7: (a) Morphology of vesicle membrane (red) enclosing two liquid droplets. The upper droplet contains the PEG-rich α phase, the lower one contains the dextran-rich β-phase. The interface (blue) between the droplets meets the membrane along the three-phase contact line, with the exterior phase denoted by γ. The two membrane segments and the interface define three (effective) contact angles, θ_α, θ_β, and θ_γ that can be directly measured by optical microscopy; (b) These contact angles and the interfacial tension $\Sigma_{\alpha\beta}$ of the (αβ) interface determine the two membrane tensions $\hat{\Sigma}_{\alpha\gamma}$ and $\hat{\Sigma}_{\beta\gamma}$.

Interfacial Phenomena

Polymer Brushes consisting of diblock copolymers undergo micro-phase separation and provide surfaces with stable nanoscale patterns, which can be used to control the organization of nanoparticles into larger aggregates as studied by the group of *C. Seidel*. Using dissipative particle simulations, a variety of different morphologies for these aggregates has been identified as well as morphological transitions, which resemble wetting transitions of liquid droplets at chemically patterned surfaces.

Morphological wetting transitions can be induced, in a rather simple way, by increasing the volume of the liquid droplets. As a consequence, these transitions also have a strong effect on surface nucleation and lead to non-isomorphic nucleation pathways. One example for such a pathway has been studied in the context of edge melting of alkane monolayers (*H. Kusumaatmaja* et al, Phys. Rev. Lett. (2012).

Complex Systems

Most macromolecules within the living cell are continuously synthesized and degraded. Experimental data on mRNA degradation and translation have been analyzed in the group of *A. Valleriani* using stochastic modeling. In the context of mRNA degradation, it was shown that the experimentally determined decay patterns for the mRNA degradation can be used to determine the age-dependent decay rates and the life time distributions of the mRNA molecules. In the context of translation, data on ribosomal profiling have been analyzed for different growth and stress conditions.

The independent research group of *S. Klumpp* addressed the interplay of physical constraints and functional requirements in living systems, with a focus on molecular machines involved in gene expression, genetic circuits, and cellular dynamics. Genetic circuits in bacteria are intimately coupled to cellular growth because many parameters of gene expression depend on the growth rate. These dependencies have been studied for the replication control system of plasmids. Some bacteria can respond to magnetic fields via organelles called magnetosomes that contain magnetic nano-particles. Robust chain formation was found to require both magnetic interactions and active transport.

Another, more abstract class of complex systems that has been studied is provided by binary or 'spin' variables on scale-free networks with correlations between their vertex degrees. In assortative and dissortative networks, the high-degree vertices are primarily connected to other high-degree and low-degree vertices, respectively. In both cases, the networks can be decomposed into vertex layers, which are ordered at low temperatures and undergo successive phase transitions as the temperature is increased, see **Fig. 8**.

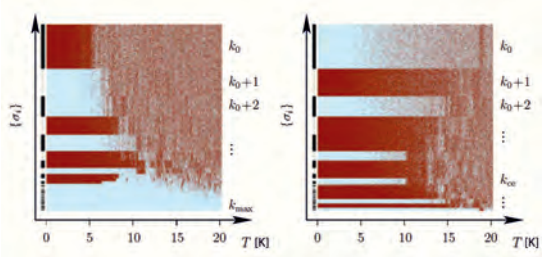

Fig 8: Typical configurations of binary or 'spin' variables on assortative (left) and dissortative (right) scale-free networks as a function of temperature T. 'Spin-up' and 'spin-down' states are shown in red and blue, respectively. Each column parallel to the y-axis shows the 'spin' states { i} of all vertices in the network. As the temperature increases, the ordered vertex layers become disordered one after another.
[J. Menche et al, Phys. Rev. E (2011)]

International Max Planck Research Schools

The department of Theory & Bio-Systems was in charge of the International Max Planck Research School (IMPRS) on "Biomimetic Systems", which was in operation from 2000 until 2012, and is also in charge of the new IMPRS on "Multiscale Biosystems", which will start in July 2013.

For additional information about research at the Department of Theory & Bio-Systems, see the following reports and www.mpikg.mpg.de/th/.

Reinhard Lipowsky
Director, Theory & Bio-Systems Department

Glycans as Universal Tools for Proteins and Lipids

Mark Santer 27.10.1971
2003: PhD in Physics at the University of Freiburg
2003-2006: Postdoc at the Institute of Microsystems Engineering, University of Freiburg. Group leader Nanofluidics
2006-2009: Employee at the Fraunhofer Institute of Mechanics of Materials (IWM), Freiburg
2009: 2010 Postdoc at the Theory Department, MPI for Colloids and Interfaces, Potsdam
From 09/2010: Group leader Carbohydrates and Polysaccharides at Theory & Biosystems Department

Carbohydrates are known to be important for cell-cell communication or in modifying the properties of proteins and lipids in the extracellular matrix. Still many of the possible biological roles of these oligosaccharides, or glycans, are yet to be elucidated. In addition to the specific recognition of many small saccharides by certain biomolecules, larger oligosaccharides have the potential to support a much broader, unspecific functionality, owing to their internal flexibility and overall diversity. For computational approaches complementing experimental studies, the latter aspects pose serious challenges, in particular at the atomistic level with respect to force field development and conformational sampling. To explore the behavior of glycans in a larger context when they are expected to fine-tune the interaction between biomolecules, a mapping onto reduced or effective models must be devised.

In our group, we currently pursue two long term case studies in order to establish a corresponding ladder of descriptions. The first study deals with the class of so-called Glycosylphosphatidylinositol(GPI)-Anchors emphasizing the interaction with lipids (with *D. Varon Silva* and *P.H. Seeberger*, Department of Biomolecular Systems, MPIKG; *C. Stefaniu* and *G. Brezesinski*, Department of Interfaces, MPIKG), and the second with specific carbohydrate-protein interactions (with *S. Barbirz*, University of Potsdam and *G. Widmalm*, University Stockholm) important for infections of gram-negative bacteria by bacteriophages.

GPI Anchors as Glycolipids

GPIs are glycans that covalently link proteins to the outer leaflet of cell membranes **[1]**. The carbohydrate part is in close proximity to both, a protein and a lipid component at the same time, see **Fig. 1**.

For the atomistic representation of the complete GPI, only the connection to the protein is available from force field databases. For the part comprising glucosamine, phosphoinsitol and the lipid (glucosamine -α1-6*myo*no-1- phosphodistearylglycerol, highlighted by the red frame in **Fig. 1**), an adaption of the force field has been developed. For complex molecules such as this, there are few opportunities to validate the force field prediction against structural data from experiment. In a joint effort, we have investigated this molecule within Langmuir monolayers of crystalline order **[2]**.

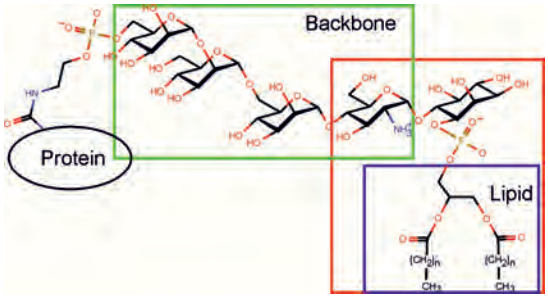

*Fig. 1.Chemical structure of a lipidated GPI molecule with protein and carbohydrate backbone. The part indicated by the red frame has been studied as a separate molecule in **[2]**.*

The Nature of the GPI Anchor Backbone

Apart from the established role as an anchoring device for proteins, there is only indirect evidence for many other possible functions of the GPI, such as being a mediator for the association of the attached protein with lipid rafts. One complication here is the heterogeneity of the molecule, its composition sensitively depends on the protein attached. For developing computational models, the invariant GPI backbone is a natural and convenient starting point. But even the seemingly basic and simple question whether this backbone is a rather flexible link or maintains a characteristic structure can only be answered comprehensively after a mapping of the atomistic to an adequate reduced model has been accomplished (**Fig. 2**). The different notions of the backbone -flexibility vs. rigidity-, can actually be reconciled by stating that the backbone assumes a rather rigid structure that can little be stretched, but is to some extent compressible by forces of physiological magnitude (starting at roughly 10pN) **[3]**.

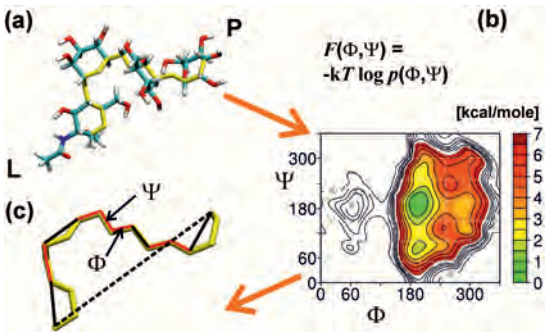

Fig. 2. (a) GPI backbone with four carbohydrate rings in stick representation. "L" and "P" indicate the direction towards the protein and the lipid, respectively. Highlighted atoms (yellow) are those retained in a reduced description. The data from all-atom MD simulations are projected onto the relevant degrees of freedom, the glycosidic torsions (c). They largely determine conformational characteristics such as the end-to-end distance (dashed line). Sugar rings are effectively represented by non-rotatable bonds (black). The free energy landscape of a corresponding pair of dihedral angles, obtained from their distribution function p, is shown in (b), reflecting the effective influence of all remaining degrees of freedom.

Do Bacteriophages Utilize the Protective Polysaccharide Coat of Gram-Negative Bacteria?

Similar questions as for the GPI emerge for certain lipopolysaccharides (LPS). Gram-negative bacteria protect themselves against invaders through a dense polysaccharide coat, which is also a target for the immune response of higher organisms invaded by these bacteria. The coat is formed by an LPS brush, the carbohydrate part of which (the O-Antigen) consists of repeating units (RU) of a tetrasaccharide building block (**Fig. 3**)

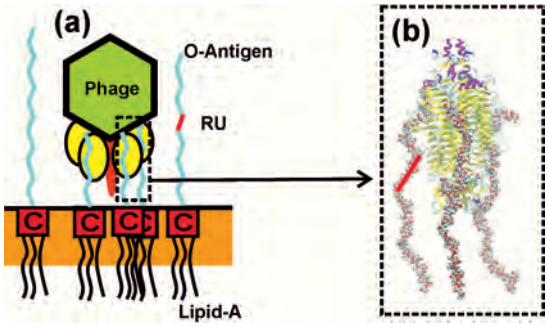

Fig. 3. (a) Schematic representation of a phage penetrating the lipopolysaccharide coat on the membrane of gram-negative bacteria. (b) snapshot of an MD simulation where three O-Antigens simultaneously attach to one tail spike protein.

A bacteriophage must, prior to infection, overcome the polysaccharide barrier before its DNA can be injected into the cell. It does so by recognizing a 2 RU epitode (an octasaccharide) with its so-called tail spike proteins (TSP), and cleaving the O-Antigen by hydrolysis at an active site on the corresponding protein scaffold. Little is known about important further aspects of the cleavage process e.g., whether it occurs continuously, is used as a means to orient the phage or to generate a force in order to push it against the membrane and initiate the DNA injection process.

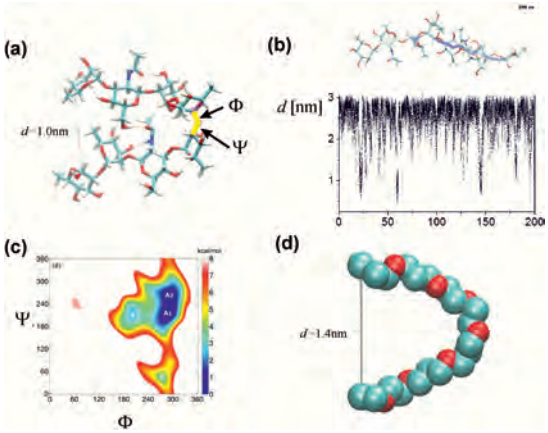

Fig. 4. (a) Hairpin-like extreme conformation of two repeat units of a serotype Y Shigella flexneri O-Antigen, the end-to-end distance of the octasaccharide can become as small as 1nm, but this event is relatively rare as shown in (b). Most of the time the molecule resided in an extended conformation as depicted above. The formation of the hairpin can be attributed to the metastable state B in the free energy landscape of the glycosidic angles, see contour plot in (c). (d) The same conformation is also observed in a reduced model similar to that in Fig. 2 (only backbone atoms are displayed).

A first clue to these questions is given by a comprehensive simulation study of short fragments (a few RU long) of the O-Antigens, see **Fig. 4**. They show the formation of hairpin-like conformations that can lead to significant temporal coiling of the otherwise stiff polysaccharide. This suggests a rich variety of carbohydrate-protein interactions, such as conformational selection of the O-Antigen by the TSP. Here we have an analogy to the interaction of a GPI anchor with a membrane. The time scales needed to characterize the problem appropriately, e.g., as transitions between many possible intermediate states, exceed the scope of atomistic simulations, and the mapping to reduced models is called for.

M. Santer, M. Wehle, Yu Kang
mark.santer@mpikg.mpg.de.

References:

[1] A. Varki et al., Essentials of Glycobiology. CSH Press, Cold Spring Harbor NY (2009).

[2] Subgel Phase Structure in Monolayers of Glycosylphosphatidylinositol Glycolipids. C. Stefaniu, I. Vilotijevic, M. Santer, D. Varon Silva, G. Brezesinski, and P. H. Seeberger, Angew. Chem. Int. Ed. http://dx.doi.org/**10.1002**/anie.201205825

[3] Mechanical Compressibility of the Glycosylphophatidylinositol(GPI) Anchor Backbone Governed by Independent Glycosidic linkages. Wehle, M.; Vilotijevic, I.; Lipowsky, R.; Seeberger, P. H.; Varon Silva, D.; Santer, M.: J. Am. Chem. Soc.http://pubs.acs.org/doi/full/**10.1021**/ja30280r

[4] Y. Kang, S. Barbirz, R. Lipowsky and M. Santer (in preparation).

Conformational Changes in Protein Function

Thomas Weikl 01.04.1970
1996: Diploma, Physics
(Freie Universität Berlin)
Thesis: Interactions of rigid membrane inclusions
1999: PhD, Physics
(Max Planck Institute of Colloids and Interfaces, Potsdam)
Thesis: Adhesion of multicomponent membranes
2000-2002: Postdoc
(University of California, San Francisco)
Since 2002: Group Leader
(Max Planck Institute of Colloids and Interfaces, Potsdam)
2008: Habilitation, Physics
(University Potsdam)
Thesis: Transition states and loop-closure principles in protein folding

Conformational Selection and Induced Changes

Protein binding and function often involves conformational changes. The changes between different protein conformations occur during binding or unbinding of ligands, or during chemical reactions of ligands that are catalysed by a protein. A central question is how the conformational changes of a protein are coupled to these binding and catalytic processes. In some cases, a conformational change has been proposed to occur predominantly prior to a binding process, an unbinding process, or a catalytic process, which has been termed 'conformational selection' since the ligand appears to select a conformation for binding, unbinding, or catalysis. In other cases, the conformational change seems to occur predominantly after a binding, unbinding, or catalytic process. The conformational change then appears to be 'induced' by this process. Binding via conformational selection implies induced-change unbinding, and vice versa, since the ordering of events is reversed in the binding and unbinding direction. The ordering of events has no effect on the binding equilibrium, but affects the binding kinetics and, thus, may be revealed by mutations that change the kinetics **[1]**. Our group has suggested a general kinetic framework that can be used (i) to identify the ordering of events in the coupling of conformational changes, binding and catalysis from mutational data and (ii) to determine the rates of the substeps of coupled processes from a combined analysis of enzyme kinetics measurements and dynamic NMR experiments that inform on the conformational exchange **[2]**.

Mutational Analysis of Binding Mechanism

Our mutational analysis of the binding and unbinding kinetics focuses on mutations distal to the binding site that mainly affect the conformational equilibrium of a protein. We find that conformational-selection processes are sensitive to such distal mutations because these processes involve a change to a low-populated, excited-state conformation prior to a binding, unbinding, or catalytic event, and because the equilibrium probability and excitation rate of this conformation depend on the conformational free-energy differences. In contrast, induced-change processes involve a conformational relaxation into a new ground state after a binding, unbinding, or catalytic event, which is rather insensitive to changes in conformational free-energy differences, provided (i) the conformational relaxation is fast **[1]**, or (ii) the transition-state for the conformational exchange is close in free energy and structure to the excited protein conformation **[2]**. The analysis of the effect of distal mutations thus can provide the basis for a simple diagnostic to identify conformational-selection versus induced-change processes.

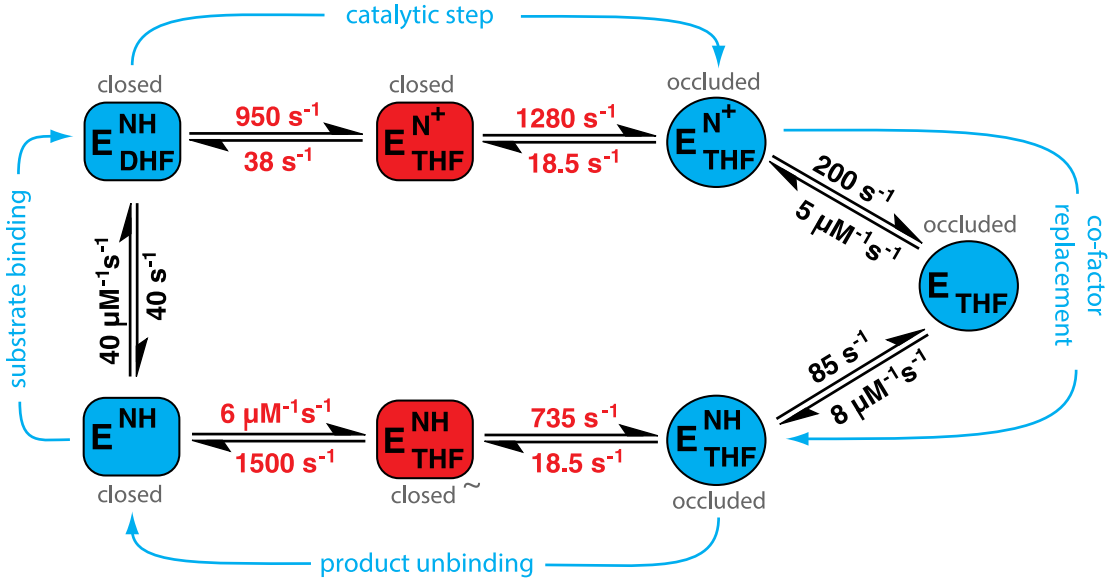

Fig. 2: Extended catalytic cycle of the enzyme DHFR from E. coli. The enzyme (E) catalyzes the reduction of dihydrofolate (DHF) to tetrahydrofolate (THF), using NADPH (NH) as a co-factor. Excited-state conformations are shown in red, ground-state conformations in blue. On our extended cycle, the catalytic step is decomposed into the actual chemical substep in the closed conformation of the enzyme required for catalysis and a physical substep in which the enzyme conformation changes from closed to occluded. Our analysis of the product-unbinding kinetics and NMR relaxation experiments indicate that the conformational change from the occluded to the closed conformation occurs largely prior to the unbinding of the product THF. Along our extended cycle, the product unbinds from an excited state with a conformation similar to the closed conformation (denoted as 'closed~').

Conformational Changes Along the Catalytic Cycle of the Enzyme DHFR

The enzyme dihydrofolate reductase (DHFR) is an important model system for investigating the interplay of conformational dynamics, binding and catalysis. DHFR from E. coli exhibits characteristic changes between a 'closed' and an 'occluded' conformation of the active-site loop along its catalytic cycle (**Fig. 1**). The change from the closed to the occluded conformation occurs during the catalytic step. Since the catalysed reaction can only occur in the closed conformation, we have suggested an induced-change mechanism in which the chemical reaction precedes the conformational change during the catalytic step (**Fig. 2**). We have determined the rates of these two substeps from experimental data for the overall rates of the catalytic step and for the rates of the conformational exchange. Our analysis of mutational data indicates that the conformational change during product unbinding follows a conformational-selection mechanism, i.e. the conformational change occurs predominantly prior to unbinding **[2]**.

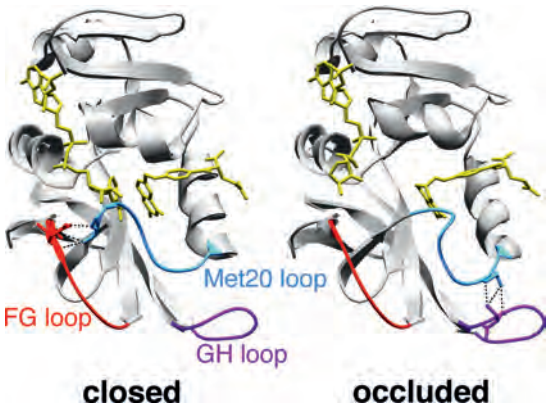

Fig. 1: DHFR from E. coli exhibits changes between a closed and occluded conformation along its catalytic cycle. In these conformations, the Met20 loop either closes over the active site, or protrudes into it. The different conformations are stabilized by different hydrogen bonds to adjacent loops. The bound substrate and co-factor here are shown in yellow.

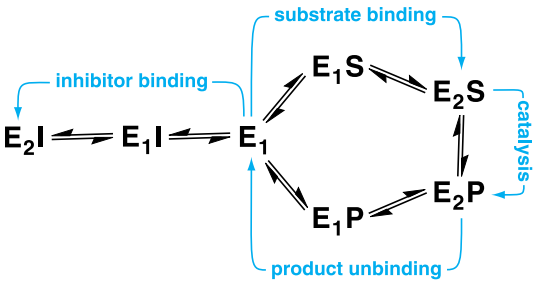

Fig. 3: 7-state model for catalysis and inhibition of an enzyme with induced-fit binding mechanism. In this model, substrate molecules S and inhibitor molecules I first bind in conformation E_1 of the enzyme. These binding events induce changes into conformation E_2 in which the substrate S is converted into the product P.

Catalysis, Inhibition and Drug Resistance of Enzymes with Induced-fit Binding Mechanism

We have extended classical models of enzyme catalysis and inhibition by including a conformational change during the binding and unbinding of substrate, product, or inhibitor molecules (**Fig. 3**). Our focus was on enzymes with induced-change binding mechanism since many enzymes close rather tightly over substrate or inhibitor molecules during binding. Binding via an induced-change mechanism, i.e. prior to the change from the 'open' to the 'closed' conformation of these enzymes, is required if the entry and exit of the ligand molecules is sterically obstructed in the closed conformation. The role of the conformational changes for catalysis and inhibition can be revealed by distal, non-active-site mutations that slightly shift the conformational equilibrium, but do not interfere directly with binding and catalysis in the active site of the enzymes. Several groups have suggested that such shifts in the conformational equilibrium might explain why non-active-site mutations can contribute to multi-drug resistance, i.e. to an increase of catalytic rates in the presence of different inhibitory drugs. Based on our extended model for enzymes with induced-change binding mechanism shown in **Fig. 1**, we have investigated how these mutations affect catalysis and inhibition **[3]**. Two cases can be distinguished: In case 1, the maximum catalytic rate of the enzyme is limited by the unbinding of the product. We find that the catalytic rate in the presence of inhibitors depends exponentially on the mutation-induced change $\Delta\Delta G_C$ of the free-energy difference between the two conformations of the enzyme in this case. Non-active-site mutations with $\Delta\Delta G_C>0$ that slightly destabilize the closed conformation 2 relative to the open conformation 1 of the enzyme lead to an increase in the catalytic rate, irrespective of the inhibitor. Such non-active-site mutations thus contribute to a multi-drug-resistance of the enzyme. In case 2, the maximum catalytic rate of the enzyme is limited by the forward rate of the catalytic step. In this case, mutation-induced changes of the conformational equilibrium have no effect on the catalytic rate in the presence of inhibitors. A comparison with experimental data for the non-active-site mutation L90M of the HIV-1 protease indicates that this enzyme appears to follow case 1, which implies that non-active-site mutations that slightly destabilize the closed conformation contribute to multi-drug resistance.

T. Weikl, B. Hemmateenejad, F. Paul
thomas.weikl@mpikg.mpikg.mpg.de

References:

[1] Weikl, T. R., and von Deuster, C.: Selected-fit versus induced-fit protein binding: Kinetic differences and mutational analysis. Proteins **75**, 104-110 (2009).

[2] Weikl, T. R., and Boehr, D. D.: Conformational selection and induced changes along the catalytic cycle of E. coli DHFR. Proteins **80**, 2369-2383 (2012).

[3] Weikl, T. R., and Hemmateenejad, B.: How conformational changes can affect catalysis, inhibition and drug resistance of enzymes with induced-fit binding mechanism such as the HIV-1 protease. Biochim. Biophys. Acta (2013).

Cargo Transport by Teams of Molecular Motors: Elastic Coupling and Interference Regimes

Florian Berger 06.11.1981
2008: Diploma, Physics, (University of Stuttgart)
Thesis: Optimization in Driven Systems
2012: PhD, Physics, (MPI of Colloids and Interfaces, Potsdam) Thesis: Different Modes of Cooperative Transport by Molecular Motors
Since 2012: Postdoc (MPI of Colloids and Interfaces, Potsdam)

Corina Keller 27.10.1977
2009: Diploma, Physics, (Humboldt University Berlin)
Thesis: Coupled Molecular Motors
2013: PhD, Physics, (MPI of Colloids and Interfaces, Potsdam) Thesis: Coupled Molecular Motors: Network Representation and Dynamics of Kinesin Motor Pairs
Since 2013: Postdoc (MPI of Colloids and Interfaces, Potsdam)

Active transport by molecular motors is ubiquitous in all eukaryotic cells. These motor proteins convert chemical energy into mechanical work which enables them to transport cargoes such as RNAs, protein complexes or organelles. Such intracellular transport is often driven cooperatively by several molecular motors, which may belong to the same or to different motor species like kinesin, dynein or myosin. These motors step stochastically along filaments, from which they unbind after a finite run length. Understanding how these motors interact and how their movements are coordinated and regulated is a central and challenging problem of cellular transport **[1]**. To establish a general theoretical framework for elucidating and analysing such transport processes, we recently introduced two complementary approaches: (i) a detailed enzymatic chemo-mechanical description that starts from the nucleotide states of the single motors **[2]** and (ii) a coarse-grained description considering the single motor as a stochastic stepper **[3,4]**. Such theoretical approaches integrate the well-established properties of individual motors into a predictive theory for cooperative transport.

Network Representation of Motor Pairs

Cargo transport by two coupled molecular motors is studied using a chemomechanical network for the complete transport system and analyzing the trajectories generated by this network. The theoretical description starts from the different nucleotide states of a single motor supplemented by chemical and mechanical transitions between these states. As an instructive example, we focus on kinesin-1, for which a detailed chemomechanical network has been developed previously **[5]**. The motor pair system considered here consists of two kinesin motors, a leading and a trailing motor, which are attached to the same cargo and walk on the same filament. Each motor can unbind from and rebind to the filament individually. As a consequence, the cargo is actively pulled by either one or two motors. A mechanical step of one of the motors during a 2-motor run leads to an elastic interaction force between the two motors described by the extension of a linear spring. The state space of the elastically coupled motor pair is characterized by three variables, the chemical states i_{le} and i_{tr} of the leading and trailing motor and of the extension ΔL of the motor-motor separation **[2]**. The resulting network has a layer structure as shown in **Fig. 1**, where each layer corresponds to a constant value of ΔL. Any 1-motor run occurs on one of the boundary lines of the network and may be terminated either by unbinding of the active motor which leads to the unbound motor pair state, or by the rebinding of the inactive motor and a subsequent 2-motor run. Mechanical steps during 2-motor runs lead to transitions between neighbouring ΔL-layers. Even though this motor pair network has a complex structure, it involves, apart from the single motor parameters, only two additional parameters, the coupling parameter K and the single motor rebinding rate π_{si}.

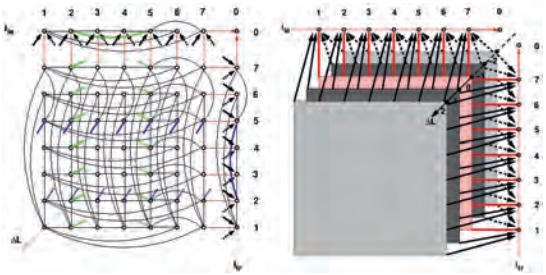

Fig. 1: State space of a motor pair described by the individual motor states i_{le} and i_{tr} and the extension ΔL of the motor-motor separation. (left) Detailed description of the layer with ΔL=0 and (right) stack of five ΔL-layers.

Activity States and Motor Pair Parameters

In stochastic simulations, we studied the trajectories generated from the chemomechanical network of the motor pair as a function of the single motor rebinding rate π_{si} and the elastic coupling parameter K **[2]**. In experimental studies, the values of these two parameters are usually not known but have to be determined in a consistent manner. Our theory shows that one can determine these two parameters by measuring the average run times during 1- and 2-motor runs of cargo trajectories. Alternatively, individual motor trajectories and the properties of the ΔL-distribution can be used to deduce the two unknown parameters. Which activity state is dominant during a motor pair walk also depends on these two parameters. The corresponding activity diagram in **Fig. 2** shows the crossover line which separates the parameter regime, in which 1-motor runs dominate the cargo run, from the regime, in which 2-motor runs are more likely. From individual motor trajectories, one can deduce the distribution of the extension ΔL of the motor-motor separation during 2-motor runs as shown in **Fig. 2**. Within the studied range for the coupling parameter, the number of accessible ΔL values varies by one order of magnitude. The maximal values of ΔL observed in the simulations determines the size of the network in **Fig. 1**.

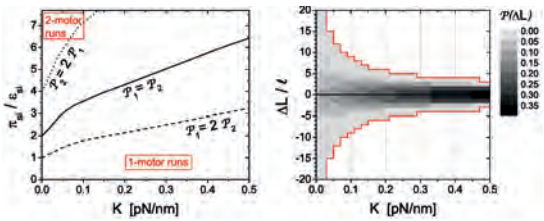

Fig. 2: (left) Activity regimes of a motor pair as a function of elastic coupling parameter K and single motor rebinding rate π_{si}. (right) Probability distribution P(ΔL) for the extension ΔL of the motor-motor separation as a function of the coupling parameter K.

Distinct Transport Regimes for Elastically Coupled Motors

The case of cargo transport by two identical motors involves an elastic coupling between the motors that can reduce the motors' velocity and/or the binding time to the filament. We show that this elastic coupling leads, in general, to four distinct transport regimes characterized by the motor pair's average velocity v_2 and its average binding time t_2, during which the two motors remain simultaneously bound to the filament **[3]**. Both quantities depend on the single motor dynamics and on the strength K of their elastic coupling. Thus, strongly coupled and/or fast motors can quickly build up a large strain force that pulls one of the motors from the filament, while weakly coupled and/or slow motors may unbind spontaneously before reaching such a large force. The motor pair dynamics are governed by the interplay of three different forces: the stall force F_s, which corresponds to the maximal force that a single motor can generate, the detachment force F_d, which is the typical force that one motor can sustain for an extended period of time, and the scale F_K for the elastic strain forces between the two motors.

Using a continuous-time Markov process to describe the single motors as stochastic steppers, we calculate the average binding time t_2 and the velocity v_2 for two active motors and identify four different transport regimes, see **Fig. 3**. We estimate the crossover lines between these regimes from time scale arguments for the strain force generation which, in addition, allows us to obtain an intuitive understanding of the mutual motor-motor interference.

We apply our framework to predict the behavior of different pairs of molecular motors based on typical parameters from single motor experiments. In addition to a weak coupling regime, kinesin and dynein motors are found to exhibit a strong coupling and an enhanced unbinding regime, whereas myosin motors are predicted to attain a reduced velocity regime. All of these regimes can be explored experimentally by varying the elastic coupling parameter K. Our theory is consistent with the available experimental data for a kinesin-1 and myosin V.

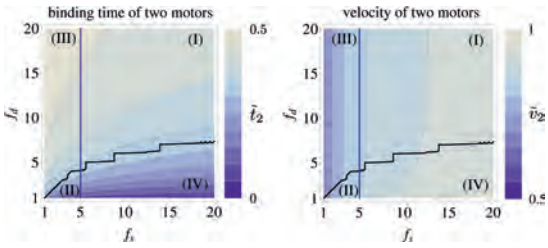

Fig. 3: (left) Average binding time and (right) velocity of a cargo pulled by two active motors in units of the single motor binding time and single motor velocity, respectively. Both quantities are displayed in a colored contour plot as functions of the rescaled single motor stall force $f_s=F_s/F_K$ and the rescaled detachment force $f_d=F_d/F_K$, where the force scale $F_K=K/2l$ is the elastic strain force between the motors per motor step with step size l. The solid blue line separates the region with and without a reduced velocity, whereas the solid black line separates the region of spontaneous and force-induced unbinding. These lines define four distinct transport regimes: (I) weak coupling with essentially unchanged velocity and binding time; (II) strong coupling with both reduced binding time and reduced velocity; (III) reduced velocity with no effect on the binding time and (IV) enhanced unbinding with no effect on the velocity.

F. Berger, C. Keller, S. Klumpp, R. Lipowsky
florian.berger@mpikg.mpg.de.
corina.keller@mpikg.mpg.de

References:

[1] Berger, F., Keller, C., Müller, M. J. I., Klumpp, S., Lipowsky, R., Co-operative transport molecular motors, Biochem. Soc. Trans., **39**, 1211-1215 (2011).

[2] Keller, C., Berger, F., Liepelt, S., Lipowsky, R., Network complexity and parametric simplicity for cargo transport by two molecular motors, J. Stat. Phys., **150**, 205-234 (2013).

[3] Berger, F., Keller, C., Klumpp, S., Lipowsky, R., Distinct transport regimes of two elastically coupled molecular motors, Phys. Rev. Lett., **108**, 208101 (2012).

[4] Berger, F., Keller, C., Lipowsky, R., Klumpp, S., Elastic coupling effects in cooperative transport by a pair of molecular motors, Cell. Mol. Bioeng., 6, 48-64 (2013).

[5] Liepelt, S., Lipowsky, R., Kinesin's network of chemomechanical motor cycles, Phys. Rev. Lett., **98**, 258102 (2007).

Depolymerization of Actin Filaments

Thomas Niedermayer 18.12.1981
2008: Diploma, Physics (University of Marburg); Thesis: Synchronization, phase-locking, and metachronal wave formation in ciliary chains
2012: PhD, Physics (MPI of Colloids and Interfaces, Potsdam); Thesis: On the depolymerization of actin filaments
Since 2012: Postdoc (MPI of Colloids and Interfaces, Potsdam)

Actin is one of the most abundant and highly conserved proteins in eukaryotic cells. The globular protein assembles into long filaments, which form a variety of different networks within the cytoskeleton. The dynamic reorganization of these networks – which is pivotal for cell motility, cell adhesion, and cell division – is based on cycles of polymerization (assembly) and depolymerization (disassembly) of actin filaments. Actin binds adenosine triphosphate (ATP), and within the filament the actin-bound ATP is hydrolyzed into adenosine diphosphate (ADP) on a time scale of a few minutes.

Because ADP-actin dissociates faster from the filament ends than ATP-actin, it was thought that the filament becomes less stable as it grows older. However, recent depolymerization experiments with single filaments suggested the opposite behavior. Abrupt dynamic changes during filament depolymerization have been observed in buffers containing no free monomers, and indicate that the actin filaments become increasingly stable with time. Several mechanisms for this stabilization have been proposed. The most prominent hypothesis correlates the stabilization with structural transitions of the whole filament helix **[1]**.

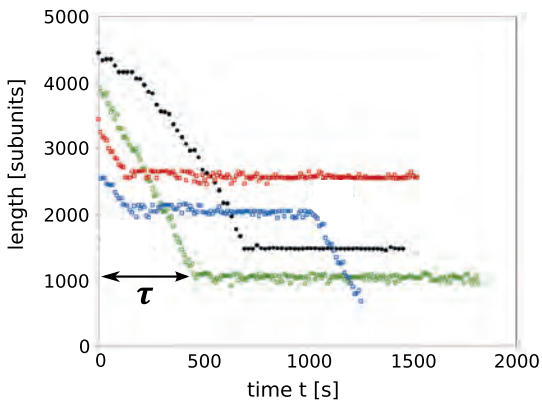

Fig. 1: Length of four actin filaments as a function of time. The filaments depolymerize in buffers containing no free monomers. The shrinkage is suddenly interrupted at a certain interruption time , which differs from filament to filament and represents a stochastic variable.

Interruptions of Depolymerization

In order to study the interruptions of depolymerization, we collaborated with the experimental lab of Marie-France Carlier in Gif-sur-Yvette (France). A combination of single filament microscopy and stochastic modeling allowed us to discover the surprising mechanism of filament stabilization **[2,3]**. In depolymerization experiments on filaments having one end blocked, we confirmed that filaments abruptly cease to shrink and determined the time from the initiation of depolymerization until the occurrence of the first interruption, see **Fig. 1**. This duration time τ differs from filament to filament and represents a stochastic variable.

We considered various hypothetical mechanisms that may cause the observed interruptions. These mechanisms cannot be observed directly, but they lead to distinct distributions of the duration τ and these distributions can be compared with those obtained from single filament experiments. By modeling the underlying stochastic processes – such as the association and dissociation of filament subunits and putative transformations of these subunits – we computed the cumulative distribution functions $P(t) = \text{prob}(\tau \leq t)$ of the stochastic variable τ for all transformation mechanisms in question. For global filament transformations, which were implicitly considered in **[1]**, or transitions that only occur at the depolymerizing filament end, the duration τ is exponentially distributed. Furthermore, many other mechanisms – for instance the copolymerization of actin with already transformed subunits – give rise to an approximately exponential distribution of τ. Successive transformations of subunits starting from a single seed cause the duration τ to have a very narrow Gaussian distribution, and thus result in a sharp rise of P(t) at $t = \langle\tau\rangle$. For the experimentally relevant range of parameters, local transformations of random subunits within the filament lead to a cumulative distribution that is well described by the expression

$$P(t) = 1 - \exp(-\alpha\omega t^2), \qquad (1)$$

where the parameter α is fixed by both the polymerization and depolymerization velocities, and the free parameter ω is the rate of the putative subunit transformations. A comparison of our analytical expressions with the measured distribution, see **Fig. 2**, revealed that the sudden truncation of the shrinkage process does neither arise from blocking of the ends nor from a collective transition of the whole filament. Instead, we have predicted a novel, local transition process occurring at random sites within the filament.

The combination of additional single filament experiments with our theoretical approach – and in particular with a generalization of the distribution in equation (1) – confirmed the notion of a local transition mechanism and identified the postulated transition as the photo-induced formation of an actin dimer within the filaments. Furthermore, we showed that only fluorescently labeled filament subunits may exhibit a transition and that unlabeled actin filaments do not exhibit pauses. This implies that, *in vivo*, older filaments become destabilized by ATP hydrolysis, in contrast to the view expressed in **[1]**.

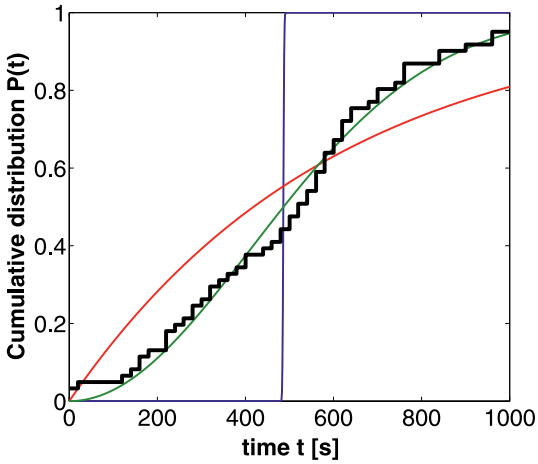

Fig. 2: The cumulative distribution P(t) = prob ($\tau \leq t$) of the duration τ, i.e., the probability that the interruption occurs at any time prior to time t, provides a fingerprint of the mechanism that causes the interruption. The exponential distribution (shown in red) is implied by many possible mechanisms such a transformations that may occur only at the shrinking filament end. The step-like function (shown in blue) is caused by sequential transformations of the filament subunits. Local transformations of random subunits lead to a cumulative distribution given by equation (1) and displayed in green. Experimental data are shown in black. The red, blue, and green curves corresponding to theoretical distributions were obtained by least-square-fitting of the respective distributions to the experimental distribution. Each fitting procedure involves only one fit parameter provided by the transition rate ω. Since the data can only be described by the green curve, we conclude that the interruptions arise from local transitions of random subunits within the filament. As soon as such a transformed subunit arrives at the shrinking end, it causes the interruption of depolymerization.

Mechanism of ATP Hydrolysis

The filament destabilization by ATP hydrolysis becomes apparent as an acceleration of the depolymerization prior to the interruption: In **Fig. 1**, the black data, corresponding to a filament grown from ATP-actin, exhibit an increase of the depolymerization velocity, whereas the red, green and blue data points, obtained for three filaments grown from ADP-actin, exhibit shrinkage with constant velocity. The mechanism of ATP hydrolysis has remained elusive for many years: Both the so called "random model", where ATP is hydrolyzed at each subunit with the same rate, as well as the "vectorial model", where ATP hydrolysis exclusively takes place at a subunit neighboring an ADP-actin subunit, have been proposed in the literature. The measurement of the time-dependent depolymerization velocity using fluorescence microscopy in conjunction with a theoretical description of the depolymerization process and a careful data analysis reveals that the rate of ATP hydrolysis is constant within the filament, corresponding to a random hydrolysis mechanism **[3,4]**. This method also provided novel insight into the function of profilin, a protein that accelerates actin depolymerization in cells, thus demonstrating the method's potential in the functional analysis of actin regulators.

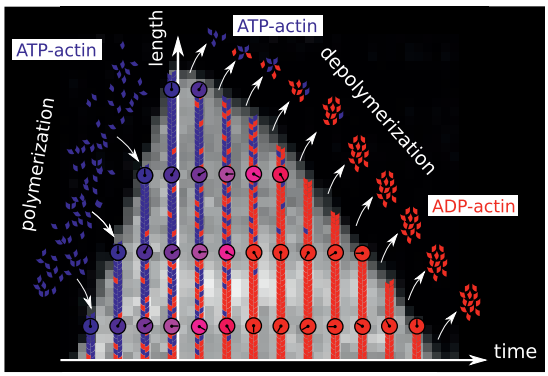

Fig. 3: The time-dependent extension of an actin filament is shown in light gray. Left of length axis: During polymerization, ATP-actin is incorporated into the filament. The subsequent hydrolysis of the bound ATP gives rise to ADP-actin. Right of length axis: The velocity of depolymerization increases over time, since ADP-actin dissociates more rapidly from the filament end than ATP-actin. The local composition of the filament (i.e. the fraction of ATP-actin) can be inferred from the time-dependence of the depolymerization velocity and is indicated by the coloring of the small clocks. These clocks measure the `age' of the subunit at the respective position within the filament, that is the time that has elapsed since the incorporation of the respective filament segment. The correspondence between the color of the clocks and the local time indicates that the rate of ATP hydrolysis is constant along the filament.

Thomas Niedermayer, Reinhard Lipowsky
thomas.niedermayer@mpikg.mpg.de

References:

[1] Kueh, H. Y. and Mitchison, T. J. Structural plasticity in actin and tubulin polymer dynamics. Science **325**, 960-963 (2009).

[2] Niedermayer, T., Jégou, A., Chièze, L., Guichard, B., Helfer, E., Romet-Lemonne, G., Carlier, M.-F. and Lipowsky, R. Intermittent depolymerization of actin filaments is caused by photo-induced dimerization of actin protomers. Proc. Natl. Acad. Sci. USA **109**, 10769-10774 (2012).

[3] Niedermayer, T. PhD Thesis: On the depolymerization of actin filaments (2012).

[4] Jégou, A., Niedermayer, T., Orbán, J., Didry, D., Lipowsky, R., Carlier, M. and Romet-Lemonne, G. Individual actin filaments in a microfluidic flow reveal the mechanism of ATP hydrolysis and give insight into the properties of profilin. PLoS Biology **9**, e1001161 (2011).

Stability of Lipids and Lipid Bilayers

Andrea Grafmüller 18.08.1980

2000-2004: Master in Science (MSci), Physics (1st Class Honours), Queen Mary University of London. Thesis: Computer Simulation of Kinetic Ising Systems with Glauber Dynamics

2004-2007: Doctoral Thesis: The Fusion of Membranes and Vesicles (Max Planck Institute for Colloids and Interfaces)

2007-2009: Postdoctoral Scientist Department of Theory and Bio systems, Max Planck Institute of Colloids and Interfaces.

2009-2010: Postdoctoral Scientist, University of Utah

2010-2011: Postdoctoral Scientist, University of Chicago

2011-2012: Research Scientist, Department of Theory and Bio systems, Max Planck Institute of Colloids and Interfaces.

Since 2012: Research Group Leader, Department of Theory and Bio systems, Max Planck Institute of Colloids and Interfaces

Lipid bilayers belong to the most important structural elements of biological cells. For biological function, a flexible and dynamic internal structure and membrane composition is required. Thus, despite their great inherent stability, the lipid membranes constantly undergo remodeling processes, involving membrane fusion, pore formation and various means of lipid exchange between membranes.

Understanding the molecular mechanisms and energetics that govern such remodeling processes presents a great challenge for both experiments and molecular modeling. This challenge arises from the disparate length and time scales involved. Bilayer membranes have lateral sizes of 100 nm to over 100 µm, yet are only a few nanometers in thickness. The processes of interest take place or are initiated at the scale of one or at most a couple of lipids molecules, i.e. a few nanometers. At the same time, they take place on time scales too fast for high resolution experiments, yet are non-equilibrium processes, and out of reach for most molecular simulations.

Strategies to overcome these difficulties involve either the use of simplified coarse-grained models, with fewer degrees of freedom as used in **[1-3]** to study membrane fusion, or enhanced sampling methods, such as umbrella sampling, which forces the system out of equilibrium, along a chosen reaction coordinate. Here we describe the application of the latter strategy to two membrane related processes.

Energetics of Nano-Pore Formation

Pore formation plays an important role in many cellular processes that require membrane remodeling, as well as for biomedical applications.

Theories of pore formation are often based on classical nucleation theory as a balance between the edge energy and the membrane tension Σ. When the pore radius is close to the molecular scale however, this continuum description is unlikely to hold, because the creation and closure of the hydrophobic pore requires considerable rearrangement of the lipid molecules at the pore edge.

Simulation studies of pore formation are limited to small length and time scales, and thus require artificially large membrane tensions. Alternatively, the free energy required to create a nm sized hydrophilic pore can be calculated with umbrella sampling. Here, the chosen reaction coordinate was the distance z of a certain lipid head group from the bilayer's center of mass.

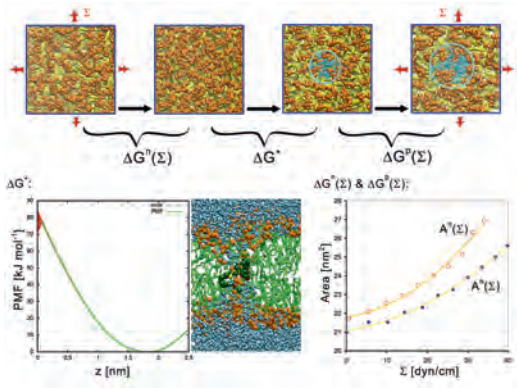

Fig.1: Scheme for calculating the free energy of pore formation as a function of membrane tension in simulated lipid bilayers.

When the headgroup is close to the center of the bilayer a pore forms spontaneously and the corresponding potential of mean force (PMF) can be calculated. This method is however computationally expensive and limited to individual values of membrane tension. A scheme to estimate the pore formation free energy as a function of tension Σ is outlined in **Fig. 1**. In this scheme the process of creating a pore in a bilayer at a given Σ is devided into three steps: 1) reducing the bilayer tension from Σ to zero, 2) creating a nano-pore and 3) stretching the bilayer containing a pore back to Σ.

Using this scheme, the free energy of pore formation has been calculated as a function of Σ. The validity of the results can be tested by comparing the results to a second PMF calculation at a high lateral pressure of -40 bar, which finds the pore formation free energy to be 61.7±3 kJ mol^{-1}. In comparison, the integration scheme leads to a value of 64±4 kJ mol^{-1}, demonstrating, that this method gives reliable results, over a large range of membrane tensions.

The results can be used to estimate the probability of finding a nanopore in a membrane as a function of membrane tension and size. The tensions for which this probability reaches finite values of ~10% correlate well with the order of magnitude of rupture tensions observed for simulated membrane patches and typical vesicle sizes, despite the different timescales. A fit of the pore free energy as a function of Σ for the line tension gives a value of 7.2 pN, which is close to experimental estimates ranging from 8 to 21 pN **[4]**.

As the restrained lipid influences the pathway of pore formation, it is not a priori clear that unrestrained conditions lead to the same intermediate transition states for pore formation. It is not possible to observe the formation of nanopores in unrestrained simulations, but simulations of nanopore closing can give insights to the intermediate con-

formations. The two, very similar closing pathways are shown in **Fig. 2**. The first proceeds via a half-pore, spanning one of the monolayers only and is the same as the one observed in the pore formation pathway of the restrained simulations. In the second case, instead of a half-pore in one monolayer, two smaller hydrophilic indentations are present in both monolayers. A full hydrophobic pore spanning the entire bilayer is never seen.

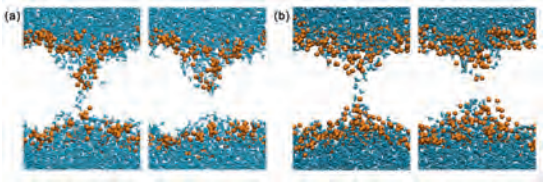

Fig 2: Two possible intermediate states observed in pore closing simulations. (a) a 'half-pore' spanning one monolayer (b) two smaller hydrophilic indentations, one in eachmonolayer.

Lipid Exchange and Local Geometry

Similar PMF calculations, restraining the lipid head-group at a range of distances outside the bilayer membrane can be used to estimate the desorption free energy **[5]**.

For a tension-free membrane the desorption free energy is found to be 63±2 kJ mol^{-1}. Using the same protocol to determine the free energy change upon desorption of a lipid from a tense bilayer with a lateral pressure of -40 bar, we find a desorption free energy of 80±2 kJ mol^{-1}, 17 kJ mol^{-1} larger than for the desorption from the relaxed bilayer. To understand this difference, the different contributions to the free energy change have to be considered. The major contribution will be the energy cost of exposing the hydrophobic tails to the water. However, when the lipid is pulled into solution, its tails, which are extended within a conical region in the bilayer, become disordered with random orientations, as in **Fig. 3c**, increasing their conformational entropy. This represents a favorable contribution to lipid desorption and partially compensates the hydrophobic interactions. In the tense bilayer, the lipids are more disordered and therefore gain less entropy in solution. To investigate this effect of the local structure further, the free energy of desorption of a lipid from a spherical micelle has also been calculated. Due to the high local curvature the lipid tails in the micelle are even more disordered than in the tense bilayer. As expected, the desorption free energy for the micelle is also higher than for the tension-free bilayer, with 73±1.3 kJ mol^{-1}.

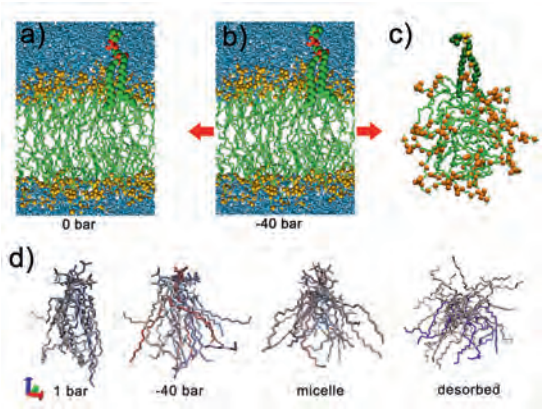

Fig.3: Three different aggregates, for which the desorption free energy has been calculated (a-c). (d) The conformational space of individual lipids within the three aggregates and in solution.

For a more quantitative assessment, the average conformational entropy of lipid tails in the different aggregates has been estimated with the quasi-harmonic (QH) approximation. The results are summarized in Table 1. In the tense membrane, the change in conformational entropy of 14±5 kJ mol^{-1} provides a quantitative explanation for the difference in desorption free energy. The difference in conformational entropy in the spherical micelle, on the other hand, with 55±5 kJ mol^{-1} is significantly larger than that in the desorption free energies, which only differ by ~10 kJ mol^{-1}. Therefore, the large lipid entropy change is to a large part compensated by other free energy contributions. This result is consistent with the observation, that the number of tail–water contacts for a lipid chain in the micelle is approximately 5 times as high as in the membrane aggregates, leading to a reduced contribution of water–chain interactions.

What has become clear from studying these three systems is that the local structure has a strong influence on the free energy of lipids in the aggregates.

	ΔG^{des} (kJ/mol)	$\Delta\Delta G^{des}$ (kJ/mol)	$T\Delta\Delta S$ (kJ/mol)
Bilayer P_{II} =0 bar	63 ±2	0	0
Bilayer P_{II} =40 bar	80 ±2	17 ±3	14±5
Micelle	73 ±1.3	10 ±3	55 ±5

Table.1: The free energy for lipid desorption, ΔG^{des} for the transfer of a DPPC lipid from an aggregate into water, the difference from the bilayer at zero tension, $\Delta\Delta G^{des}$ and the change in lipid entropy in the aggregates relative to the bilayer at zero tension, $-T\Delta\Delta S$

A. Grafmüller, V. Knecht, R. Lipowsky
gmueller@mpikg.mpg.de.

References:

[1] Grafmüller, A., J. Shillcock, and R. Lipowsky, Physical Review Letters, . **98**(21) (2007).

[2] Grafmüller, A., J. Shillcock, and R. Lipowsky, Biophysical Journal, **96**(7): p. 2658-2675 (2009).

[3] Grafmüller, A., J. Shillcock, and R. Lipowsky, Molecular Simulation, **35**(7): p. 554-560 (2009).

[4] Portet, T. and R. Dimova, Biophysical Journal, **99**: p. 3264-3273 (2010).

[5] Grafmüller, A., R. Lipowsky, and V. Knecht, Physical Chemistry Chemical Physics, **15**(3): p. 876-881 (2013).

Lipid Membranes in Contact with Aqueous Phases of Polymer Solutions

Rumiana Dimova 06.04.1971
1991-1995: Master of Science majoring in Theoretical Chemistry and Chemical Physics (Sofia University, Bulgaria)
1996-1997: Second Master of Science majoring in Physical Chemistry (Sofia University, Bulgaria)
1997-1999: Doctoral Thesis: Hydrodynamic properties of model lipid membranes: study by means of optical trapping manipulation of particles. (Bordeaux University, Centre de Recherche Paul Pascal, Bordeaux, France)
2000-2001: Postdoctoral Scientist, Theory Department, Max Planck Institute of Colloids and Interfaces
Since 2001: Research Group Leader, Department of Theory and BioSystems, Max Planck Institute of Colloids and Interfaces

The interior of living cells is crowded with macromolecules and organelles. The weight fraction of proteins, RNAs and polysaccharides is on the order of 20–30 %. Interactions between macromolecules in water can lead to the formation of coexisting aqueous phases. Thus, in the concentrated interior of the cell, local phase separation may occur, involving microcompartmentation, which in turn can affect, e.g., cell functioning and the performance of cytoplasmic proteins.

The phenomenon of phase separation is often observed in solutions of two polymer species. The most well studied aqueous two-phase system (ATPS) formed by macromolecules is the one of poly(ethylene glycol) (PEG) and dextran. We studied the phase separation of this system in the closed compartment of lipid vesicles as a model for biological microcompartmentation. Giant lipid vesicles loaded with polymer solutions typically contain two droplets with different polymer compositions, formed by phase separation within the vesicle interior **[1]**. We employed these cell-sized biomimetic systems to study the wetting behavior of the polymer phases on the membrane **[2, 3]**, the reorganization of the lipid bilayer arising from molecular crowding **[4]** and the resulting morphological shapes adopted by vesicles loaded with ATPS **[5]**.

Aqueous Two-Phase Polymer Solutions of Dextran and PEG

Above a total polymer weight fraction of a few weight percent, aqueous solutions of PEG and dextran demix. The corresponding two-phase region is bounded by the binodal line within the phase diagram of the system (**Fig. 1**). At concentrations below the binodal the polymer solution is homogeneous. Above the binodal, the solution undergoes phase separation and the compositions of the coexisting phases are given by the tie lines in the phase diagram. A variety of methods for tie-line determination has been explored in the literature based on the use of different experimental techniques. Recently, we proposed a relatively simple approach based on density measurements of the phases **[6]**.

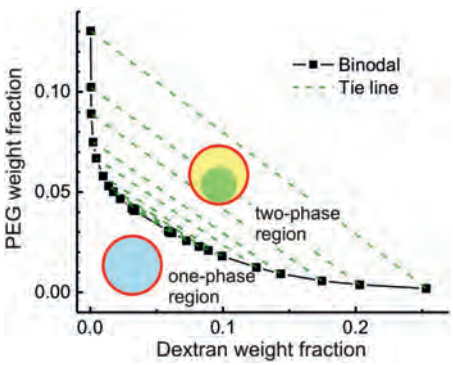

*Fig. 1: Binodal and tie lines of the aqueous solution of dextran (molecular weight 400-500 kg/mol) and PEG (molecular weight 8 kg/mol) measured at 24 °C **[6]**. Below the binodal the polymer solution is homogeneous; above the binodal it undergoes phase separation. The insets schematically illustrate the vesicle membrane (red) enclosing the homogeneous solution (blue) or the two liquid droplets consisting of dextran-rich (green) and PEG-rich (yellow) phases.*

Membrane Wetting and Wetting Transition

Liquid droplets at interfaces may exhibit zero or nonzero contact angles corresponding to complete or partial wetting, respectively. As one varies the liquid composition, the system may undergo a transition from complete to partial wetting. Such a transition can also occur for an aqueous solution enclosed within a vesicle **[2]**. In this case, the substrate is the lipid membrane.

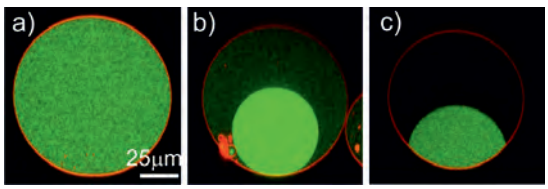

Fig. 2: Phase separation inside a vesicle (confocal vertical cross-sections). The membrane is labelled in red; a small fraction of dextran is labelled in green. As the external osmolarity is increased in a stepwise manner, phase separation occurs (a, b) and the dextran-rich drop (green) undergoes a wetting transition (b, c).

We used giant vesicles encapsulating PEG-dextran solutions in the one-phase state (**Fig. 2a**). In order to obtain vesicles containing two phases, we raise the interior polymer concentration above the binodal by exposing the vesicles to a hypertonic medium, i.e., by osmotic deflation. The polymer concentration inside increases, leading to phase separation (**Fig. 2a, b**). The dextran-rich phase is heavier and thus, the dextran-rich droplet is always located at the bottom of the vesicle. When the external osmolarity is further increased, the dextran-rich phase starts to wet the membrane (**Fig. 2c**). The morphology change of the dextran-rich droplet indicates a wetting transition from complete wetting of the PEG-rich phase in **Fig. 2b** to partial wetting in **Fig. 2c**.

Wetting-Induced Budding

When both phases wet the membrane, the smaller one may bud out of the vesicle upon further deflation (**Fig. 3a-c**). Initially, for weak deflation, the vesicle is approximately spherical (**Figs. 2c and 3b**). Upon further deflation, the dextran-rich phase starts to form a bud away from the PEG-rich phase (**Fig. 3c**). The excess area arising from deflation is utilized by the vesicle to undergo morphological changes and a budding transition **[5]**. The direction of budding can be reversed if the phase separation occurs in the vesicle exterior **[5]**.

In mechanical equilibrium, the two membrane tensions $\hat{\Sigma}_{pe}$ and $\hat{\Sigma}_{de}$ must be balanced along the contact line (where the external medium, the PEG-rich phase and the dextran-rich phase are in close proximity) by the interfacial tension Σ_{pd} between the two liquid phases (**Fig. 3d**). The interfacial tension Σ_{pd} pulls on the membrane towards the vesicle interior. When Σ_{pd} is small, the membrane tensions can easily balance this pulling force in the normal direction and the contact angle θ_e remains close to 180 degrees. As the interfacial tension Σ_{pd} increases and the vesicle is deflated further, the membrane tension can no longer sustain the quasi-spherical vesicle shape, the membrane bends along the contact line and the dextran-rich phase buds out. The budding event sig-

nificantly reduces the interfacial energy by decreasing the interfacial area between the two liquid phases.

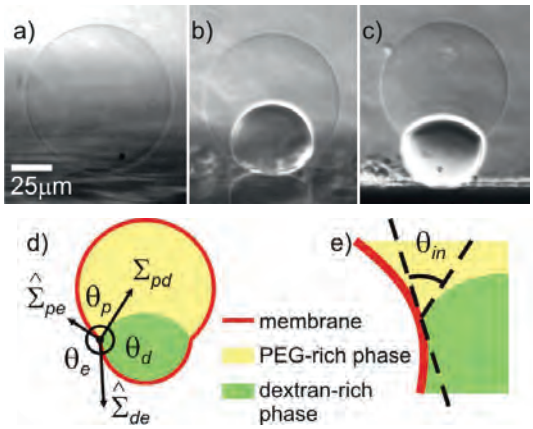

Fig. 3: (a-c) Side-view phase contrast images of a budding vesicle. After phase separation (a, b), the interior solution consists of PEG-rich (lighter) and dextran-rich (heavier) droplets. Further deflation of the vesicle causes the dextran-rich droplet to bud out as shown in (c). In the sketch in (d), the three effective contact angles as observed with optical microscopy are indicated as well as the two membrane tensions and the interfacial tension Σ_{pd}. The intrinsic contact angle θ_{in}, which characterizes the wetting properties of the membrane by the PEG-rich phase at the nanometer scale is sketched in (e).

The kink in the vesicle membrane shown in **Fig. 3c, d** is observed by optical microscopy but cannot persist to small length scales, since such a kink would imply an infinite bending energy of the membrane. Therefore, when viewed with suboptical resolution, the membrane must be smoothly curved as in **Fig. 3e**, which implies the existence of an intrinsic contact angle θ_{in}. In contrast to the three contact angles shown in **Fig. 3d**, the intrinsic contact angle represents a material parameter that is independent of the vesicle geometry **[3]**.

Formation of Membrane Nanotubes

Upon vesicle deflation, excess area is created. Depending on the membrane tension and spontaneous curvature, the area created during deflation may lead to vesicle budding as shown above, and/or may be involved in creating membrane nanotubes **[4]**, which have a diameter below optical resolution and become visible when fluorescently labelled (**Fig. 4**). The tubes form during the phase separation process and are stable after this process has been completed. They are always in contact with the PEG-rich phase and adsorb onto the two-phase interface forming a layer or meshwork of tubes (**Fig. 4b**). When the interface becomes overcrowded, hundreds of tubes protrude into the PEG-rich phase (**Fig. 4c**).

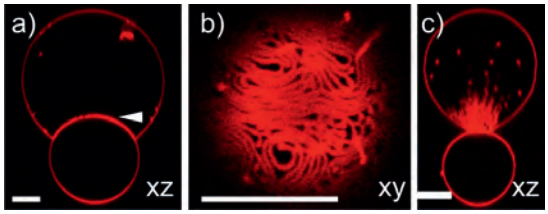

Fig. 4: Tube formation in vesicles with internal phase separation. (a) Vertical xz-section showing adsorption of tubes onto the two-phase interface (arrowhead). (b) Horizontal xy-section at the z-position of the arrowhead in (a) showing tubes at the two-phase interface. (c) Vertical xz-section of a vesicle with overcrowded two-phase interface; the tubes protrude into the upper PEG-rich phase. The scale bars correspond to 15 µm.

A theoretical analysis of the deflated vesicles reveals that these membrane tubes are stabilized by negative spontaneous curvature **[4, 7]**. Using the large separation of length scales between the tube diameter and the overall size of the vesicles, the spontaneous curvature can be calculated and is found to be about –1/(240 nm) for a certain range of polymer concentrations. The nanotubes can also be retracted back into the mother vesicle by increasing the membrane tension via micropipette aspiration of the vesicle.

R. Dimova, H. Kusumaatmaja, Y. Li, R. Lipowsky, Y. Liu
dimova@mpikg.mpg.de.

References:

[1] Dimova R. and Lipowsky R., Soft Matter, **8**, 6409-6415 (2012).
[2] Li Y., Lipowsky R. and Dimova R., J. Am. Chem. Soc., **130**, 12252-12253 (2008).
[3] Kusumaatmaja H., Li Y., Dimova R. and Lipowsky R., Phys. Rev. Lett., **103**, 238103 (2009).
[4] Li Y., Lipowsky R. and Dimova R., Proc. Natl. Acad. Sci. U.S.A., **108**, 4731-4736 (2011).
[5] Li Y., Kusumaatmaja H., Lipowsky R. and Dimova R., J. Phys. Chem. B, **116**, 1819-1823 (2012).
[6] Liu Y., Lipowsky R. and Dimova R., Langmuir, **28**, 3831-3839 (2012).
[7] Lipowsky R., Faraday Discussions, **161**, 305-331 (2013).

Interplay of Curvature and Composition in Membranes

Thomas Weikl 01.04.1970
1996: Diploma, Physics
(Freie Universität Berlin)
Thesis: Interactions of rigid membrane inclusions
1999: PhD, Physics
(Max Planck Institute of Colloids and Interfaces, Potsdam)
Thesis: Adhesion of multicomponent membranes
2000-2002: Postdoc
(University of California, San Francisco)
Since 2002: Group Leader
(Max Planck Institute of Colloids and Interfaces, Potsdam)
2008: Habilitation, Physics
(University Potsdam)
Thesis: Transition states and loop-closure principles in protein folding

Biological membranes are the 'skin' of our cells and cell organelles. They consist of a large variety of different lipids and proteins, and are highly flexible and fluid, which allows drastic changes in membrane shape and curvature. The interplay of molecular composition and curvature of the membranes is crucial for their biological function. Our group investigates this interplay during the encapsulation of nanoparticles **[1]**, in the formation of membrane domains **[2]**, and upon membrane adhesion **[3]**.

Cooperative Wrapping of Nanoparticles

Recent advances in nanotechnology have led to an increasing interest in how nanoparticles interact with biological matter. While biomedically designed nanoparticles are promising carriers for drug delivery, the wide application of industrial nanoparticles has also led to concerns about their safety. To enter the cells or cell organelles of living organisms, nanoparticles have to cross biomembranes. The membranes deform and wrap around nanoparticles if the adhesive interaction between the nanoparticles and membranes is sufficiently strong to compensate for the cost of membrane bending. While the wrapping of single nanoparticles by membranes has been studied intensively in theory and simulations, relatively little is known about the organization and elastic, membrane-mediated interactions of multiple nanoparticles adsorbed on membranes. These interactions arise because the elastic deformations of membranes depend on the distance between the adsorbed particles.

Our group has recently found strongly attractive elastic interactions between spherical nanoparticles adsorbed on vesicles **[1]**. These attractive interactions lead to bound states of the particles with a morphology that depends on the ratio of the area and volume of the vesicles, which is typically characterized by the reduced volume $v \leq 1$. The maximal value $v = 1$ of the reduced volume corresponds to the area to volume ratio of a sphere. For large values of v, nanoparticles are only partially wrapped by the vesicle since the area to volume ratio does not allow full wrapping. For such values of v, we have found bound states in which two particles are equally wrapped by the vesicle (**Fig. 1a**). For smaller values of v, we have found strongly bound states in which two or more particles are cooperatively wrapped by a membrane tube that protrudes into the vesicle (**Fig. 1b and c**). This tubular confinement of several nanoparticles constitutes a novel route to encapsulate nanoparticles reversibly in vesicle membranes. In experiments, the amount of confined nanoparticles as well as their release may be controlled by changes in the osmotic conditions, which lead to changes in the reduced volume of the vesicles.

The wrapping and membrane-mediated interactions of the nanoparticles arise from the interplay of membrane bending and adhesion. The total energy is the sum of the bending energy of the vesicle and the overall adhesion energy of the particles. We have determined the minimum total energy of the vesicle and particles with simulated annealing Monte Carlo simulations of triangulated vesicles in contact with particles. In **Fig. 2**, the minimal total energy E of a vesicle with two adsorbed particles is displayed as a function of the particle distance r. At the reduced volume $v = 0.96$, the total energy E(r) exhibits local minima at the contact distance $r = 2R_p$ of the particles and at a distance r between $6R_p$ and $9R_p$, separated by an energy barrier. The local minimum of E at the contact distance $r = 2R_p$ corresponds to the bound state of the particles shown in **Fig. 1a** in which both particles are symmetrically wrapped by the vesicle membrane. At $v = 0.92$ and 0.94, we find additional branches of low-energy conformations with negative values of E at distances $r < 3\ R_p$ of the particles. In these low-energy conformations, the particles are jointly but asymmetrically wrapped by a membrane tube that invaginates into the vesicles (**Fig. 1b** and snapshot at bottom left of **Fig. 2**). In these conformations, the wrapping of the particles is asymmetric since the particle at the tip of the invagination is more strongly wrapped. Besides these low-energy conformations, we have found branches of higher-energy conformations with positive values of E in which the particles are symmetrically wrapped as in **Fig. 1a**. In addition, we have investigated the adhesion of membranes via adsorbed nanoparticles **[4]**.

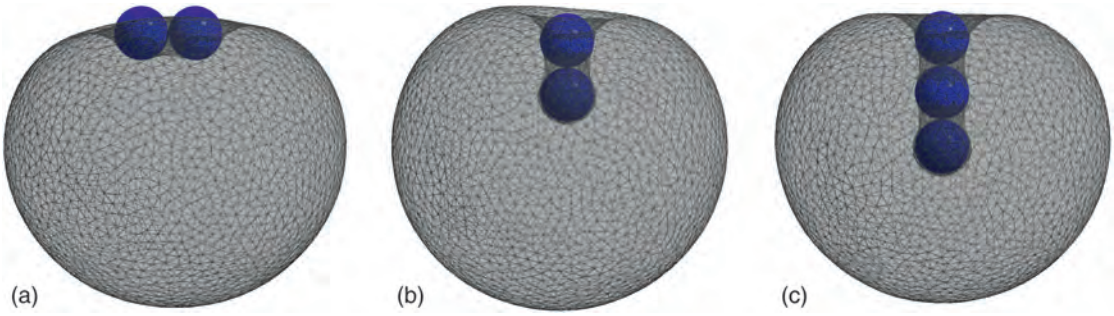

Fig. 1: (a) Bound state of two particles for the reduced volume $v = 0.96$ of the vesicle and the rescaled adhesion energy $u = U R_p^2/\kappa$ of the particle where U is the adhesion energy per area, R_p is the particle radius, and κ is the bending rigidity of the vesicle membrane. - (b) Strongly bound state of two particles for $v=0.92$ and $u=2.33$. - (c) Strongly bound state of three particles for $v = 0.88$ and $u = 2$. In (b) and (c), the particles are jointly wrapped by a membrane tube that protrudes into the vesicle.

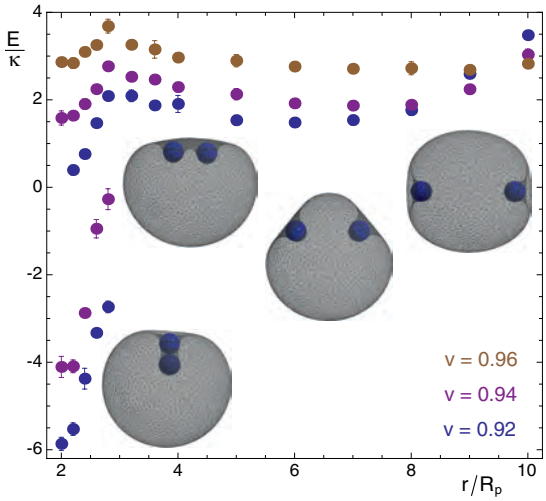

Fig. 2: Minimal total energy E of a vesicle with two adsorbed particles as a function of the particle distance r for the rescaled adhesion energy u=2.33 and the values v=0.92, 0.94, and 0.96 of the reduced volume. The minimal total energy E is given in units of the bending rigidity κ of the membrane. The particles with radius R_p are in contact at the distance $r=2R_p$. The four snapshots represent minimum energy conformations for the reduced volume v=0.92 at particle distances with r/R_p = 2, 3.2, 6 and 9.

Vesicles with Multiple Lipid Domains

Multicomponent lipid vesicles with coexisting liquid-ordered and liquid-disordered domains are widely used as model system for the lipid bilayers of cells. The liquid-ordered domains have a significantly higher bending rigidity than the liquid-disordered domains. Our group has investigated the coupling of curvature and composition of vesicles that contain such domains **[2]**. We have modeled these vesicles as triangulated surfaces, and have determined their equilibrium morphologies with Monte Carlo simulations. The total energy of the vesicles is the sum of the overall bending energy of the vesicle and the line energy of the domains. We have found that the interplay between the bending energies of the domains and the line energy of the domain boundaries can lead to multi-domain morphologies in which the flexible liquid-disordered domains are located in more strongly curved sections of the vesicles (**Fig. 3**).

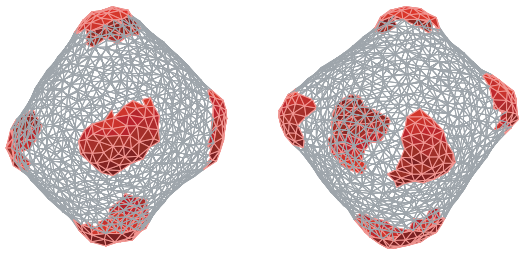

Fig. 3: Stable multi-domain morphologies of vesicles with coexisting liquid-ordered (grey) and liquid-disordered domains (red). In these morphologies, the more flexible liquid-disordered domains are located at more strongly curved 'edges' of the vesicle.

Protein Domains in Cell Adhesion Zones

Submicron scale domains of membrane-anchored receptor proteins play an important role in cell signaling. Central questions concern the stability of these microdomains, and the mechanisms leading to the domain formation. In immune-cell adhesion zones, microdomains of short receptor-ligand complexes form next to domains of significantly longer receptor-ligand complexes. The length mismatch between the receptor-ligand complexes leads to membrane deformations and has been suggested as a possible cause of the domain formation. The domain formation is a nucleation and growth process that depends on the line tension and free energy of the domains. Our group has derived general expressions for the line tension between domains of long and short receptor-ligand complexes and for the adhesion free energy of the domains with a combination of analytical calculations and Monte Carlo simulations **[3]**. We have found that the length mismatch of receptor-ligand complexes alone is sufficient to drive the domain formation, and have obtained submicron-scale minimum sizes for stable domains that are consistent with the domain sizes observed during immune-cell adhesion.

T. Weikl, A. H. Bahrami, J. Hu, H. Krobath, T. Stieger, G. Xu
thomas.weikl@mpikg.mpg.de.

References:

[1] Bahrami, A. H., Lipowsky, R., and Weikl, T. R.: Tubulation and aggregation of spherical nanoparticles adsorbed on vesicles. Phys. Rev. Lett. **109**, 188102 (2012).

[2] Hu, J., Weikl, T. R., and Lipowsky, R.: Vesicles with multiple membrane domains. Soft Matter **7**, 6092-6102 (2011).

[3] Krobath, H., Rozycki, B., Lipowsky, R., and Weikl, T. R.: Line tension and stability of domains in cell-adhesion zones mediated by long and short receptor-ligand complexes. PLoS ONE **6**, e23284 (2011).

[4] Stieger, T., Schoen, M., and Weikl, T. R.: Adhesion of surfaces mediated by adsorbed particles: Monte Carlo simulations and a general relationship between adsorption isotherms and effective adhesion energies. Soft Matter **8**, 11737 (2012).

Anchored Polymers – Self-Organization & Response to Perturbations

Christian Seidel 07.02.1949
1972: Diploma, Physics (Technical University Dresden) Thesis: Calculation of angular distribution and polarization of nucleon scattering close to resonance energies
1978: Dr. rer. nat., Polymer Physics (Institute for Polymer Chemistry, Teltow) Thesis: On the calculation of the phonon dispersion of solid polymers, application to polyvinylidenfluoride
1979-83: Research Scientist (Ioffe Physico-Technical Institute, Leningrad)
1983-89: Research Scientist (Institute for Polymer Chemistry, Teltow)
1985: Dr. sc. nat., Solid State Theory (Institute for Polymer Chemistry, Teltow) Thesis: Ground states and critical temperatures in quasi-one-dimensional systems
1989-91: Group Leader (Institute for Polymer Chemistry, Teltow)
Since 1992: Group Leader (Max Planck Institute of Colloids and Interfaces, Potsdam)
1994: Habilitation, Theoretical Chemistry (Technical University, Berlin)

Assembly of Nano-Particles at AB Diblock Copolymer Brushes

Polymer brushes, i.e., polymers densely anchored to an interface have received much interest because of their scientific and technological importance. Brushes consisting of incompatible components are of special interest because they exhibit phase separation on nanometer scales. Lateral segregation can lead to stable surface nano-patterns that can be used to control the organization of nano-particles (NP) into larger aggregates.

To study both the morphology of diblock copolymer brushes (DCB) and the organization of nanoparticles we use dissipative particle dynamics (DPD) simulation **[1, 2]**. In our model, there are five different types of DPD beads: polymer A and B blocks (A, B), solvent (S), nanoparticles (P), and wall (W). The interaction strength between these beads is set by the DPD parameters a_{ij}. Polymer chains are anchored via the ends of soluble A blocks while the solvent is poor for B blocks. Under such conditions, A blocks form stretched brushes whereas insoluble B blocks exhibit different morphologies, which depend both on solvent quality and chain composition $f_B = N_B / (N_A + N_B)$, where $N_{A,B}$ are the lengths of A and B blocks, respectively.

We performed an extensive simulation study of the morphology diagram of such polymer brushes, where the AB immiscibility and solvent selectivity are treated independently and on an equal footing **[1]**. Such an approach, which is a natural extension of the standard model of DCBs, seems to be necessary to obtain results that are consistent with experimental data of, e.g., polystyrene-polymethylmethacrylate brushes.

Morphological Changes Caused by B-like Nano-particles

B-like nano-particles (e.g., core particles covered by a polymer B shell) exhibit high affinity to polymer B domains. At low NP load, particles follow the various brush pattern and form ordered spherical aggregates or extended chains depending on both polymer composition f_B and NP concentration φ. With increasing φ, we observe morphological transitions of the microphase-separated DCB resulting in a shift towards structures appearing in pure DCBs only at larger f_B values (**Fig. 1**). Such a behavior is very similar to that previously obtained for diblock copolymer melts.

Spreading of Nano-droplets along Polymer Stripes

Considering B-unlike nano-particles we observe a strong tendency that NPs aggregate into a single, large droplet, which is mostly located on the top of a B domain. Hexagonally ordered many-droplet morphologies are only obtained for relatively weak incompatibility between nano-particles and polymer B. On the other hand, we demonstrated that spreading along B stripes can be realized if (i) the surface tension at the droplet-solvent interface is reduced and (ii) the contrast between polymer B affinities of NPs and solvent is sufficiently strong (**Fig. 2**) **[2]**. The observation of two different spreading regimes, i.e., complete spreading of NPs along B stripes

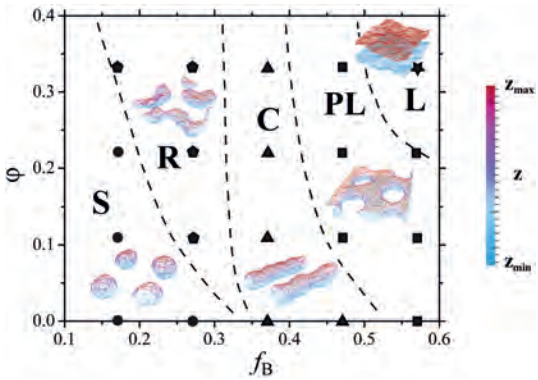

Fig. 1: Morphology diagram of AB diblock copolymer brushes mixed with B-like nano-particles in the (f_B, φ)- parameter space. The five different phases of B domains, i.e., spherical (S) and cylindrical (C) micelles, ripple-like (R), perforated (PL) and complete (L) lamella, are illustrated by characteristic snapshots where the color-coding indicates the distance from the grafting plane. Symbols indicate simulation points.

or localization into one large droplet, agrees qualitatively quite well with theoretical predictions about wetting morphologies on substrates with striped surface domains **[3]**.

Furthermore, our study suggests a new mechanism to move nano-objects on the surface of diblock copolymer brushes. A slight change of the NP's solvophobicity can alter the equilibrium position of the droplet from the top of a B domain (**Fig. 2B, g**) to the valley between two neighboring domains (**Fig. 2B, h**). Performing additional simulations we have shown that the particular process is reversible. The new mechanism relies only on a switching of the solvophobicity of nano-particles, which, in principle, can be realized by covering them with appropriate pH-sensitive ligands.

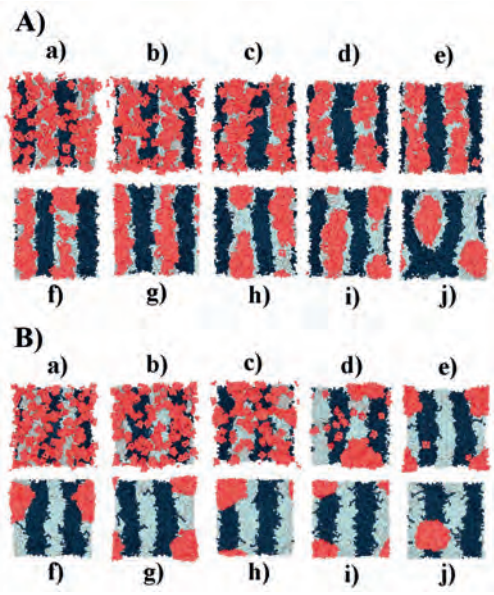

Fig. 2: Spreading of B-unlike nano-particle along B stripes for increasingly insoluble NPs from a_{PS} = 26 (a) to 37 (j) (f_B = 0.37, φ = 0.224, a_{AB} = a_{PA} = 40). Anchored A blocks are colored dark blue, B blocks light blue and nano-particles red. A) a_{PB}=27, B) a_{PB}=35.

Field-regulated Force by Grafted Polyelectrolytes

During the past couple of decades, investigations of the response of charged polymers, so-called polyelectrolytes, to external electric field attracted much scientific attention. If the free end of a grafted polyelectrolyte is under load, while the chain itself is exposed to electric field that favors its adsorption, both field strength and force determine the configuration of the chain. In particular, a restoring force may arise if the chain is mechanically coupled to a deformable, nano-sized object such as another polymer chain or a colloidal particle. In that case, force and length of the bulk polymer segment pulled off from the adsorption layer are determined in a self-regulated manner.

We study the response of grafted polyelectrolytes to electrostatic fields both theoretically and by means of molecular dynamics simulations. Two strictly different setups are considered. First, we apply a constant force and analyze the length of the bulk part of the chain as a function of varying electric field (**Fig. 3**) **[4]**. Note that force is measured in units of $k_BT/b \approx k_BT/l_B \approx 6$ pN and electric field in units of $k_BT/(be) \approx k_BT/(l_Be) \approx 4x10^7$ V/m, with b being the distance between charges. l_B is the Bjerrum length and e the elementary charge. Our theory is based on a detailed description of both adsorbed and bulk parts of the chain and goes beyond previous studies. **Fig. 3** demonstrates quite clearly the agreement between simulation data and theory without any fitting parameter. In addition, we observe that the length of the bulk part may be fairly well estimated by a purely mechanical theory, which accounts only for force balance and yields $f = NEe$ (**inset of Fig. 3**). Using our theory we are able to explain the surprising accuracy of the simple mechanical approach.

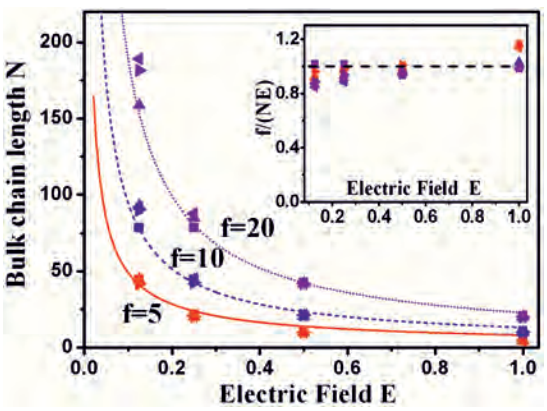

Fig. 3: Size N of the desorbed bulk part of the chain as a function of electric field E at constant pulling force f = 5, 10, and 20. (Lines – theory, symbols – simulation data.) Inset: Rescaled force f/(NE) as a function of E.

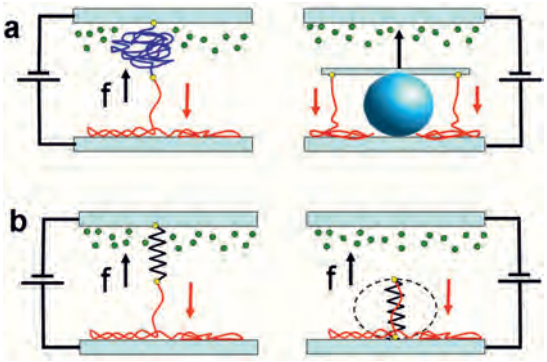

Fig. 4: (a) Two possible setups to explore field-regulated force generation. Red down arrows indicate the force generated by an electric field that favors polyelectrolyte adsorption. Black arrows show the counteracting force caused by the deformation of the linker/body. (b) The simulation setups used to model the „experimental" ones shown in the upper panel. The free chain end is linked to linear or nonlinear springs, respectively.

In the second setup, the free end of a grafted polyelectrolyte is linked to a target body. Two different models are schematically shown in **Fig. 4**. The right panel demonstrates also the working principle of a possible nano-device. We consider a few target bodies with different force-deformation relations both linear and nonlinear ones **[5]**. Among the latter we focus on the so-called Hertzian force, which mimics the behavior of a squeezed colloidal particle. The predictions of our theory agree quantitatively with the results of the numerical simulations, while a zero-order approximation that corresponds to the purely mechanical approach yields substantial deviations (**Fig. 5**).

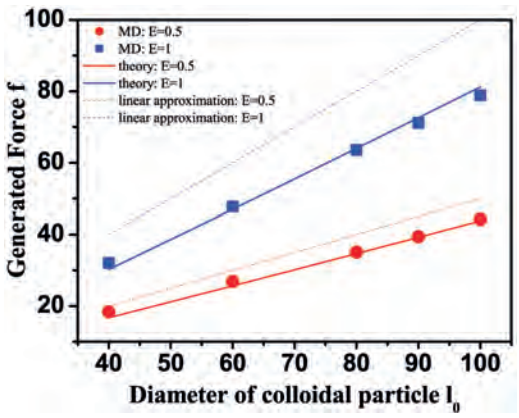

Fig. 5: The dependence of generated force f on equilibrium Hertzian spring length l_0 (size of colloidal particle). Solid lines give theoretical predictions; symbols represent simulation data while dashed lines show the results of a zero-order approximation that corresponds to the simple mechanical theory.

The project is done in collaboration with *Prof. N. V. Brilliantov*, University of Leicester.

C. Seidel, O. A. Guskova*)
seidel@mpikg.mpg.de.
*) present address: Leibniz-Institut für Polymerforschung Dresden

References:

[1] Guskova, O. A., Seidel, C.: Mesoscopic Simulations of Morphological Transitions of Stimuli-Responsive Diblock Copolymer Brushes. Macromolecules **44**, 671 (2011).
[2] Guskova, O. A., Seidel, C.: Assembly of nano-particles on diblock copolymer brushes: toward laterally nano-structured composites. Soft Matter **8**, 2833 (2012).
[3] Brinkmann, M., Lipowsky, R.: Wetting morphologies on substrates with striped surface domains. J. Appl. Phys. **92**, 4296 (2002).
[4] Brilliantov, N. V., Seidel, C.: Grafted polyelectrolyte in strong electric field under load: Field-regulated force and chain contraction. Europhys. Lett. **97**, 28006 (2012).
[5] Seidel, C., Budkov, Yu. A., Brilliantov, N. V.: Field-regulated force by grafted polyelectrolytes. J. Nanoeng. Nanosyst., to appear.

Stochastic Processes in Complex Bio-Systems

Angelo Valleriani 14.03.1966
1992: Diploma, Physics (University of Bologna)
Thesis: Conformal Invariance, Renormalization Group and Integrable Models in Two-Dimensional Quantum Field Theories
1996: PhD, High-Energy Physics (SISSA-ISAS, Trieste)
Thesis: Form Factors and Correlation Functions
1996-1998: Postdoc, (Max Planck Institute for the Physics of Complex Systems, Dresden)
1998-2000: Postdoc (Max Planck Institute of Colloids and Interfaces, Potsdam)
Since 2000: Group Leader and IMPRS Coordinator, (Max Planck Institute of Colloids and Interfaces, Potsdam)

Degradation of mRNA and Translational Control

Degradation of mRNA is one of the key processes that control gene expression in the cells. Traditionally, this process has been thought to be governed by a decay rate constant. Biochemists, however, have unveiled a large number of complex mechanisms underlying mRNA degradation. In addition, several measurements of mRNA turnover have shown that mRNA decay is rarely simple. The turnover of mRNA molecules introduces new timescales that interact with the timescales of translation and of cell division. In **[1]** we have considered the interaction of the lifetime distribution of an mRNA species with the timescale needed by ribosomes to build a stable polysome (**Fig. 1**). The latter timescale is proportional to the length of the mRNA. We have found out that for very long mRNAs with a high turnover, the transient time until protein synthesis begins may be comparable with the lifetime of the mRNA thus affecting both the protein synthesis rate and the size of the polysome.

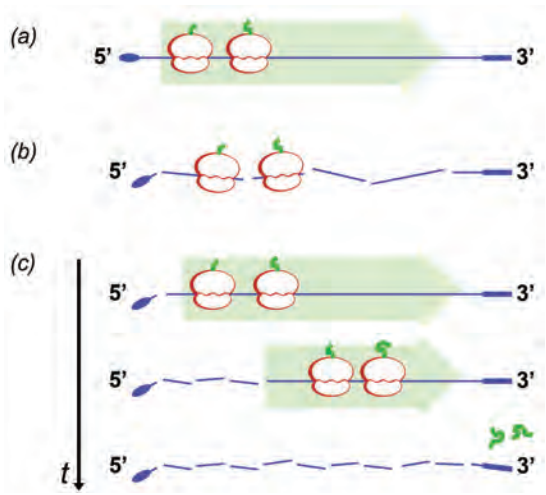

Fig. 1: Translation and degradation of mRNA. (a) Prokaryotic mRNA and (b) the effect of endonucleolitic degradation on the polysome. (c) Eukaryotic mRNA. Degradation occurs in the 5′ to the 3′ direction.

The analysis of experimental data from E. coli shows that longer mRNA produce, in general, fewer proteins than shorter mRNA if the lifetime distribution of the mRNA is short and exponential (**Fig. 2**).

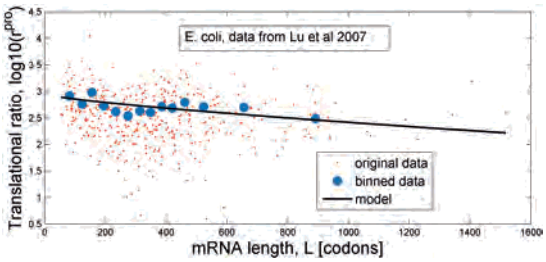

Fig. 2: The interplay between degradation and loading of the polysome can produce a negative correlation between the number of proteins per mRNA and its length.

There is also an indication that mRNA degradation may affect the spatial distribution of the ribosomes on the mRNA. This point was investigated in **[2]** using flux balance equations and stochastic simulations. Since the lifetime distribution of the mRNA is not exponential, in **[3]** we have looked at the interplay between the shape of the lifetime distribution and the timescales necessary to reach a steady state expression level (**Fig. 3**).

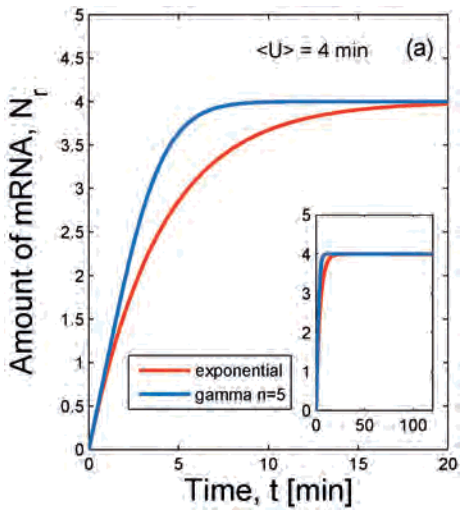

Fig. 3: Two assumptions for the mRNA lifetime distributions lead to different transient times. In E. coli the average mRNA lifetime is about four minutes and its cell cycle has duration of twenty minutes.

We found that mRNA characterized by broadly distributed lifetimes take longer to reach a steady state copy number so that especially in bacteria certain mRNAs may never reach a steady state copy number before cell division. In **[3]** we did not investigate the origin of the different lifetime distributions, a topic that was left for further investigations published in **[4]**.

Ribosomal profiling is a new experimental technique that provides an *in vivo* picture of the translational state of the cell. With this technique one can investigate the various mechanisms of translational control, which include the initiation rate by ribosomes and the codon dependent elongation rate. One important question that we wanted to address concerns the differential translational state of organisms under different growth or stress conditions. To address this ques-

tion, in the framework of the Marie-Curie ITN "NICHE" Prof Zoya Ignatova and her lab at the University of Potsdam have worked on the ribosomal profiles of *E. coli* cell cultures under four different growth conditions. The analysis of the data produced with advanced bioinformatics tools **[5]**, will be further statistically analyzed in a manuscript in preparation **[6]** to provide the most complete picture of the differential gene expression in *E. coli* so far. This data will then become a useful benchmark for modelling the interaction of ribosome with the mRNA.

Heterogeneity of Chlamy Cell Populations

Chlamydomonas reinhardtii (chlamy) is a unicellular photosynthetic alga. The cells of this organism have the special property to remain in the growth phase for a random amount of time and attain, at a population level, a relatively broad distribution of cell sizes. One consequence is that each mother cell can produce a number of daughter cells that is roughly proportional to the logarithm of its size (**Fig. 4**). Since cell volume is often considered as a proxy for the cellular metabolic state, one first objective has been to develop a model for the cell size distribution under time-independent conditions such as those created in some bioreactors. The model can be used to calculate and compare stationary distributions for the common binary and the multiple division processes **[7]**. The model has left many questions open. One biologically important question is whether the experimentally observed diversity is solely given by the stochastic nature of cell growth and division or to the heterogeneous mixture over the phases of the cell cycle. Furthermore, we wanted to investigate if the volume of the mother cells is the only determinant of the number of daughter cells.

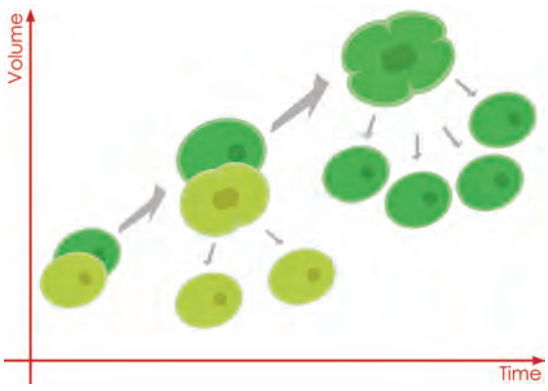

Fig. 4: Two chlamy daughter cells (bottom left) grow in time but divide at two different time points. Although the number of daughter cells is different, their sizes are very similar.

To investigate these points, Prof. Martin Steup and his lab at the University of Potsdam have performed a set of experiments with synchronized chlamy cells. The synchronization is obtained by cultivating the cells with fixed periods of light and darkness, in a growth medium that does not allow for cell growth in the darkness. Synchronization relies on the fact that, under certain general conditions, all cells would divide after the start of the dark period and the daughter cells would start to grow only when light is turned on again. Clearly, at the beginning of each light period all the cells are in the same point of the cell cycle. The experiments showed us that DNA replication occurs stochastically during the light period according to relatively simple rules that we have been able to cast in a stochastic model of cell growth and division. The conclusion of this study **[8]**, is that DNA replication is one major determinant of the number of daughter cells and that its stochastic nature maintains the population heterogeneous even under synchronization conditions.

Markov Chains in Biological Processes

Markov chains are a very common tool to mathematically model biological processes.

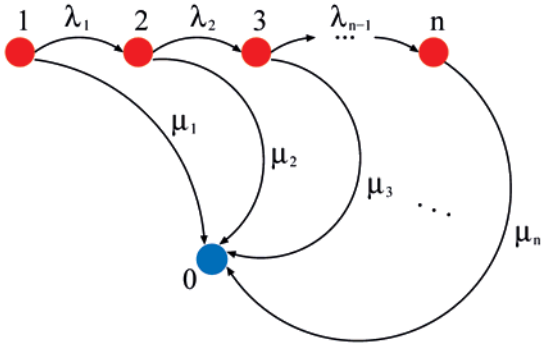

Fig. 5: The stochastic life of a single mRNA molecule is made of specific biochemical states. At each state, a transition to the next state or to absorption is possible.

The recent application of this tool in our group covers modelling the complex life time of mRNA, where each molecule undergoes several biochemical transitions until degradation takes place (**Fig. 5**, from Ref. **[4]**), and the stochastic lifetime of trabecular bones **[9]**, within a project led by Dr. Richard Weinkamer in the Biomaterials department. We have considered also mathematical models of molecular motors. In one particularly instructive work **[10]**, we have considered a simple model of molecular motors interacting with the fuel substrate. When the amount of fuel molecules is not constant, due to its stochastic consumption and replacement, the rate by which a motor receives the fuel varies stochastically in time. We could derive an analytical expression of the distribution of the time that a motor has to wait for a fuel molecule and found that it is not exponential. This implies that at low molecule number the law of mass action does not hold. Models of molecular motors like Kinesin have also inspired several problems in the mathematical theory of Markov chains that we have investigated in collaboration with Prof Sylvie Rœlly at the Institute of Mathematics of the University of Potsdam and are going to be submitted soon **[11,12]**.

A. Valleriani, C. Deneke, P. Keller, A. Nagar, M. Rading, S. Rudorf, C. Sin

References:

[1] Valleriani, A., Zhang, G., Nagar, A., Ignatova, Z., Lipowsky, R. Length-dependent Translation of Messenger RNA by Ribosomes, Phys. Rev. E **83**, 042903 (2011).

[2] Nagar, A., Valleriani, A., Lipowsky, R., Translation by Ribosomes with mRNA Degradation: Exclusion Processes on Aging Tracks, J. Stat. Phys. **145**, 1385-1404 (2011).

[3] Deneke, C., Rudorf, S., Valleriani, A., Transient Phenomena in Gene Expression after Induction of Transcription, PLoS ONE **7**, e35044 (2012).

[4] Deneke, C., Lipowsky, R., Valleriani, A., Complex degradation processes lead to non-exponential decay patterns and age-dependent decay rates of messenger RNA, PLoS ONE **8**, e55442 (2013).

[5] Zhang, G., Fedyunin, I., Kirchner, S., Xiao, C., Valleriani, A., Ignatova, Z., FANSe: an accurate algorithm for quantitative mapping of large scale sequencing reads, Nucl Acid Res **40**, e83 (2012).

[6] Fedyunin I., et al, „Global quantification of stress-response programs in bacteria with nucleotide resolution" in preparation

[7] Rading, M.M., Engel, T.A., Lipowsky, R., Valleriani, A., Stationary Size Distribution of Growing Cells with Binary and Multiple Cell Division, J Stat Phys **145**, 1-22 (2011).

[8] Sandmann, M,. Rading, M.M., et al, Single Cell Analyses and Modelling of Growth and Division of two Synchronized Chlamydomonas strains, in preparation

[9] Rusconi, M., Valleriani, A., Dunlop, J.W.C., Kurths, J., Weinkamer, R., Quantitative approach to the stochastics of bone remodeling, EPL **97**, 28009 (2011).

[10] Keller, P., Valleriani, A., Single-molecule stochastic times in a reversible bimolecular reaction, J Chem Phys **127**, 084106 (2012).

[11] Keller, P., Rœlly, S., Valleriani, A., A Quasi-Random-Walk to model a biological transport process, submitted for publication

[12] Keller, P., Rœlly, S., Valleriani, A., On Time Duality for a Quasi-Birth-and-Death-Processes, in preparation

Regulation of Bio-Processes

Stefan Klumpp 29.09.1973
1999: Diploma, Physics (University of Heidelberg)
Thesis: Noise-induced transport of two coupled particles.
2003: PhD, Physics (University of Potsdam/MPI of Colloids and Interfaces, Potsdam)
Thesis: Movements of molecular motors: Diffusion and directed walks
2004-2005: Research associate (MPI of Colloids and Interfaces, Potsdam)
2006-2009: Postdoc (University of California, San Diego)
since 2009: Group leader (MPI of Colloids and Interfaces, Potsdam)

Physical processes and interactions constrain the space of possible designs of biological systems. In addition, however, biological processes also underlie functional requirements and are the result of evolutionary selection. Our group is interested in the interplay of physical and biological forces in complex living systems, with a focus on regulatory processes, mostly in bacterial systems. We address these issues in three interrelated areas of research: (i) Molecular machines, (ii) genetic circuits, and (iii) cellular dynamics. Our main interest is in characterizing how generic physical processes enable, constrain and shape biological systems and how biological systems make use of these processes or circumvent them towards specific functions. Understanding these issues is also expected to provide theoretical guidance for applications in bioengineering and synthetic biology.

Molecular Machines

Cells contain billions of molecular machines that perform a huge variety of functions from catalysis in metabolism to processing the genetic information. Complex behaviour of such machines can arise both at the level of the properties of individual molecules and at the level of assemblies of multiple molecules **[1]**. Currently, we focus on the machines that read out the genetic information, RNA polymerases and ribosomes. Important features of these machines are proofreading mechanisms to increase their accuracy. For individual molecules, there is typically a trade-off between accuracy and speed of the read-out. Additional issues arise when many such machines process the same gene. For example, RNA polymerases have to move backward for proofreading. A trailing RNA polymerase can block this backward movement and may thus interfere with the proofreading process. If the negative effect is to be contained below a certain threshold, proofreading has to be faster than the arrival of a trailing RNA polymerase. This requirement provides a constraint on the dynamics not present for individual molecules **[2]**.

In addition to studying the mechanisms of these machines, we are interested in the economic principles that underlie their use in cells. This line of research addresses aspects such as the number of these machines present in the cell, their distribution in space, their allocation to different functions, as well as their costs and benefits for the cell. An intriguing observation in this respect is that ribosomes seem to be far more costly to the cell than RNA polymerases. The cost of ribosomes reflects the intimate coupling of the cell's ribosome content and cell growth (synthesis of biomass and proliferation), which in turn is one of the main determinants of fitness. A consequence of the fact that ribosomes represent costly investments for the cell is that using them efficiently represents a fitness advantage. One mechanism to achieve this is the usage of 'fast codons': The genetic code encodes most amino acids by several nucleotide triplets (codons), but synonymous codons may not be read out with the same rate. The use of a codon that is read out slowly incurs a fitness cost to the cell through the inefficient use of ribosomes. This fitness cost depends on how frequently the particular codon is read out. As a consequence, sequences of abundant proteins are more biased towards fast codons. We have analysed a quantitative evolution model based on this 'ribosome load' idea and derived a simple relation between the frequency of slow codons in a sequence and the abundance (copy number in the cell) of the corresponding protein **[3]**. This relation provides a simple quantitative estimate of protein abundance from sequence data alone (**Fig. 1**).

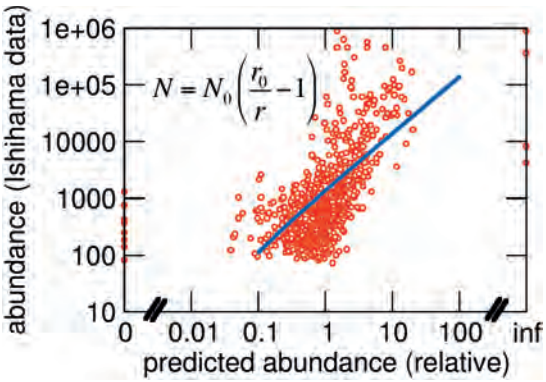

Fig. 1: Protein abundance predicted from genomic sequences: Relation between fraction of slow codons (r) and protein abundance (N) and correlation between predicted and measured abundance for E. coli [3].

Gene Regulation and Genetic Circuits

The readout of individual genes is tightly regulated in response to intracellular and external signals. Networks of genes regulating each other (via their protein products) are often compared to electronic circuits where complex functions arise from combinatorics with a limited set of basic components. This analogy is the basis for the design of synthetic gene circuits, which are then implemented on a cellular 'chassis'. However, unlike in electronics, the chassis here (the host cell) is itself a dynamic and adaptive object and the circuits are not isolated from the chassis to which they are coupled through sharing of metabolites and molecular machinery. As a consequence, changes in the state of the cell as a whole may affect individual circuits that are nominally unrelated to host cell functions. One specific example, which we have analysed recently, is the dependence of plasmid copy number on the growth rate of the host cell (**Fig. 2**). Such dependence affects the expression of all genes on the plasmid including those controlling plasmid replication, and thus its copy number. We have shown that information on such growth-rate dependencies can be used to obtain information about the design of the control system of plasmid replication **[4]**. A related issue is the systematic variation of protein concentrations that arises from the division cycle of the host cell. This variation provides a deterministic contribution to the observed 'noise' in protein synthesis **[5]**.

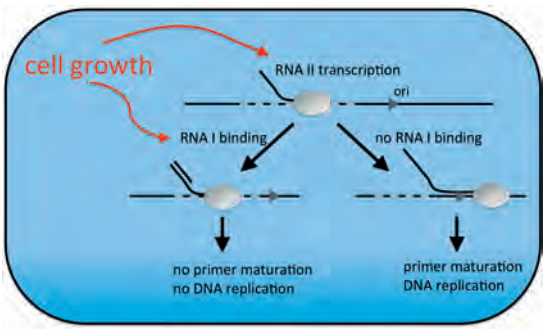

Fig. 2: Control systems of plasmid replication: Whether or not a plasmid is replicated depends on binding of a regulatory RNA (RNA I) to the replication primer (RNA II). The growth state of the host cell affects the concentrations of both RNAs.

Cellular Dynamics

In our third research area, we study the dynamics of structure formation in cells and the movements of cells. Recently we have focused on magnetotactic bacteria, in collaboration with the group of D. Faivre (Department Biomaterials). Magnetotactic bacteria orient in a magnetic field based on a chain of organelles called magnetosomes that contain magnetic nanoparticles. The magnetosome chain acts as a cellular compass needle. Magnetotactic bacteria provide an excellent model system to study what role generic physical interactions (magnetic attraction and repulsion) have in a specific biological context and how they are integrated with more specific biological mechanism. In a first project, we have studied the formation of the magnetosome chain. We developed a computer simulation based on experimental data for chain formation in iron-starved cells (**Fig. 3**). Our main question was whether the magnetic interactions between the magnetosomes are sufficient to induce chain formation. Simulations allow us to study 'in-silico mutants' defective not in individual genes, but in entire physical processes (i.e. non-magnetic mutants), which may be hard or impossible to obtain by experimental mutagenesis. The results of these simulation show that the magnetic interactions alone are not sufficient to explain the experimental observations. Rather we find that robust chain formation requires the interplay of magnetic interactions and controlled active transport **[6]**. Other topics we are currently addressing are the interactions of these bacteria with external magnetic fields and various modes of bacterial motility.

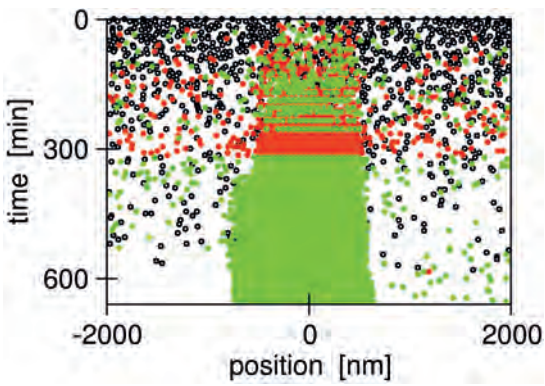

Fig. 3: Simulation of the formation of a magnetosome chain [6]: Initially non-magnetic magnetosomes (black) develop a magnetic nanoparticle (red or green indicate different directions of the magnetic moment) and align in the center of the cell with uniform magnetization.

S. Klumpp, V. Bierbaum, M. Faber, D. Gomez, M. Hintsche, R. Marathe, M. Mauri, M. Sahoo, P. Patra
klumpp@mpikg.mpg.de

References:

[1] Klumpp, S., Mechanisms and economy of molecular machines, Phys. Scr. T**151**, 014066 (2012).
[2] Sahoo, M., Klumpp, S., Transcriptional proofreading in dense RNA polymerase traffic, EPL **96**, 60004 (2011).
[3] Klumpp, S., Dong, J. J., Hwa, T., On ribosome load, codon usage and protein abundance, PLoS One **7**, e48542 (2012).
[4] Klumpp, S., Growth-rate dependence reveals design principles of plasmid copy number control, PLoS One **6**, e20403 (2011).
[5] Marathe, R., Bierbaum, V., Gomez, D., Klumpp, S., Deterministic and stochastic descriptions of gene expression dynamics, J. Stat. Phys. **148**, 607-626 (2012).
[6] Klumpp, S., Faivre, D., Interplay of magnetic interactions and active movements in the formation of magnetosome chains, PLoS One **7**, e33562 (2012).